

Towards Causal Inference for Spatio-Temporal Data: Conflict and Forest Loss in Colombia

Rune Christiansen^{†*} Matthias Baumann[‡] Tobias Kuemmerle^{‡◊}
Miguel D. Mahecha^{§¶} Jonas Peters[†]

[†]*Department of Mathematical Sciences, University of Copenhagen*

[‡]*Geography Department, Humboldt-Universitt zu Berlin*

[◊]*Integrative Research Institute on Transformations of Human-Environment Systems (IRI THESys),
Humboldt-Universitt zu Berlin*

[§]*Remote Sensing Center for Earth System Research, Leipzig University*

[¶]*German Centre for Integrative Biodiversity Research (iDiv)*

December 22, 2024

Abstract

In many data scientific problems, we are interested not only in modeling the behaviour of a system that is passively observed, but also in inferring how the system reacts to changes in the data generating mechanism. Given knowledge of the underlying causal structure, such behaviour can be estimated from purely observational data. To do so, one typically assumes that the causal structure of the data generating mechanism can be fully specified. Furthermore, many methods assume that data are generated as independent replications from that mechanism. Both of these assumptions are usually hard to justify in practice: datasets often have complex dependence structures, as is the case for spatio-temporal data, and the full causal structure between all involved variables is hardly known. Here, we present causal models that are adapted to the characteristics of spatio-temporal data, and which allow us to define and quantify causal effects despite incomplete causal background knowledge. We further introduce a simple approach for estimating causal effects, and a non-parametric hypothesis test for these effects being zero. The proposed methods do not rely on any distributional assumptions on the data, and allow for arbitrarily many latent confounders, given that these confounders do not vary across time (or, alternatively, they do not vary across space). Our theoretical findings are supported by simulations and code is available online. This work has been motivated by the following real-world question: how has the Colombian conflict influenced tropical forest loss? There is evidence for both enhancing and reducing impacts, but most literature analyzing this problem is not using formal causal methodology. When applying our method to data from 2000 to 2018, we find a reducing but insignificant causal effect of conflict on forest loss. Regionally, both enhancing and reducing effects can be identified.

1 Introduction

1.1 Spatio-temporal data analysis

In principle, all data are spatio-temporal data: Any observation of any phenomenon occurs at a particular point in space and time. If information on the spatio-temporal origin of data are available, this

*corresponding author, e-mail: krunchristiansen@math.ku.dk

information can be exploited for statistical modeling in various ways; this is the study of spatio-temporal statistics [see, e.g., Sherman, 2011, Montero et al., 2015, Cressie and Wikle, 2015, Wikle et al., 2019]. Spatio-temporal statistical models find their application in many environmental and sustainability sciences, and have been used, for example, for the analysis of biological growth patterns [Chaplain et al., 1999], to identify hotspots of species co-occurrence [Ward et al., 2015], to model meteorological fields [Bertolacci et al., 2019], or to assess the development of land-use change [Liu et al., 2017] and sea level rise [Zammit-Mangion et al., 2015]. They are frequently used in epidemiology for prevalence mapping of infectious diseases [Giorgi et al., 2018], and have also been applied in the social sciences, for example, for the modeling of housing prices [Holly et al., 2010], or for election forecasting [Pavía et al., 2008]. In almost all of these domains, the abundance of spatio-temporal data has increased rapidly over the last decades. Several advances aim to improve the accessibility of such datasets, e.g., via ‘data cube’ approaches [Nativi et al., 2017, Giuliani et al., 2019, Appel and Pebesma, 2019, Mahecha et al., 2020].

Most spatio-temporal statistical models are models for the observational distribution, that is, they model processes that are passively observed. By allowing for spatio-temporal trends and dependence structures, such models can be accurate descriptions of complex processes, and have proven to be effective tools for spatio-temporal prediction (i.e., filtering and smoothing), inference and forecasting [Wikle et al., 2019]. However, to answer interventional questions such as “How does a certain policy change affect land-use patterns?”, we require a model for the intervention distribution, that is, for data generated under a change in the data generating mechanism — we require a causal model for the data generating process.

1.2 Causality

For i.i.d. and time series data, that is, for data, for which the spatial information can be neglected, causal models have been well-studied. Among the most widely used approaches are structural causal models, causal graphical models, and the framework of potential outcomes [see, e.g., Bollen, 2014, Pearl, 2009, Peters et al., 2017, Rubin, 1974]. Knowledge of the causal structure of a system does not only provide us with cause-effect relationships; sometimes, it also allows us to quantify causal relations by estimating intervention effects from observational data. If, for example, we know that W is causing X and Y , and that X is causing Y , procedures such as variable adjustment can be used to estimate the causal influence of X on Y from i.i.d. replications from the model [Pearl, 2009, Rubin, 1974]. While using a slightly different language, the same underlying causal deliberations are the basis of many works in econometrics, e.g., work related to generalized methods of moments and identifiability of parameters [e.g., Hansen, 1982, Newey and McFadden, 1994]. In this field, data are often assumed to have a time series structure [e.g., Hall, 2005].

Existing causal models for i.i.d. or time series data do not apply easily to a spatio-temporal setting, since we cannot regard a spatio-temporal dataset as a collection of independent replications from some random vector or timeseries generated from the same underlying causal system. Nevertheless, several methods have been proposed for spatio-temporal causal modeling [e.g., Lozano et al., 2009, Luo et al., 2013, Zhu et al., 2017]. These are mostly algorithmical approaches that extend the concept of Granger causality [Granger, 1980, Wiener, 1956] to spatio-temporal data. They reduce the question of causality to predictability and a positive time lag. In particular, these methods assume that there are no relevant unobserved variables (‘confounders’) and they do not resolve the question of time-instantaneous causality between different points in space. Further, to the best of our knowledge, existing work does not provide a formal model for causality for spatio-temporal data. As a consequence, the precise definition of the target of inference, the causal effect, remains vague.

In this work, we introduce a class of causal models for multivariate spatio-temporal stochastic processes. A spatio-temporal dataset may then be viewed as a single realization from such a model, observed at discrete points in space and time. The full causal structure among all variables of a spatio-temporal process can hardly be fully specified. In practice, however, a full causal specification may also not be

necessary: we are often interested in quantifying only certain causal relationships, while being indifferent to other parts of the causal structure. The introduced causal models are well adapted to such settings. They allow us to model a causal influence of a vector of covariates X on a target variable Y while leaving other parts of the causal structure unspecified. In particular, the models accommodate largely unspecified autocorrelation patterns in the response variable, which are a common phenomena in spatio-temporal data.

The introduced framework allows us to formally talk about causality in a spatio-temporal context and can be used to construct well-defined targets of inference. As an example, we define the intervention effect ('causal effect') of X on Y . We show that this effect can be estimated from observational spatio-temporal data and introduce a corresponding estimator. We further construct a non-parametric hypothesis test for the effect being zero. Our methods do not rely on any distributional assumptions on the data generating process. They further allow for the influence of arbitrarily many latent confounders if these confounders do not vary across time. In principle, our method also allows to analyze problems where temporal and spatial dimensions are interchanged, meaning that confounders may vary in time but remain static across space.

Our work has been motivated by the following application.

1.3 Conflict and forest loss in Colombia

Tropical forests show the highest values of biodiversity for many organismic groups, e.g., in terms of vascular plants [Kreft and Jetz, 2007], or certain animal groups like amphibians [Hof et al., 2011]. Additionally, contiguous low-land tropical forests store large amounts of carbon [Avitabile et al., 2016], play an important role in climate-regulation, and provide livelihoods to millions of people [Lambin and Meyfroidt, 2011]. Yet, tropical forest loss remains a major global environmental problem, as many of these areas continue to be under pressure due to agricultural expansion [Carlson et al., 2013, Angelsen and Kaimowitz, 1999], legal and illicit mining [Sonter et al., 2017], timber harvest [Pearson et al., 2014] or urban expansion [DeFries et al., 2010].

A problem that is still only partly understood is the interaction between forest loss and armed conflicts [Baumann and Kuemmerle, 2016], which are frequent events in tropical areas [Gleditsch et al., 2002, Petterson and Wallenstein, 2015]. In particular, it has been reported that armed conflict may have both positive and negative impacts on forest loss. On the one hand, conflict can lead to increasing pressure on forests, as (illegal) timber exports may allow for financing warfare activities [Harrison, 2015]. Also, reduced law enforcement in conflict regions may lead to plundering natural resources or undertaking illegal mining activities, altogether leading to increasing forest loss [Irland, 2008, Butsic et al., 2015]. On the other hand, the outbreak of armed conflicts can also reduce the pressure on forest resources. This may happen, for example, when economic and political insecurity interrupt large-scale mining activities, or economic sanctions stopping international timber trade [Le Billon, 2000]. Investors may further be hesitant to invest in agricultural activities [Collier et al., 2000], thereby reducing the pressure on forest areas compared to peace times [Gorsevski et al., 2012]. In a global overview, Gaynor et al. [2016] call for a regional nuanced analysis of such interactions.

Along these lines, we here focus on the specific case of Colombia, where an armed conflict has been present for over 50 years, causing more than 200,000 fatalities, until a peace agreement was reached in 2016. Throughout this period, a variety of interacting social and political factors have regionally led to internal migration and changes in livelihoods and land-use that are all related to the overall conflict [Armenteras et al., 2013]. There is evidence that forest loss can be, at least regionally, attributed to the armed conflict [Castro-Nunez et al., 2017, Landholm et al., 2019]. At the same time, there are also arguments suggesting that the pressure on forests was partially reduced when armed conflict prevented logging [Dávalos et al., 2016], either directly (by demanding human resources) or indirectly (e.g., due to land-abandonment in the wake of local conflicts [Sánchez-Cuervo et al., 2012, Negret et al., 2017]). Most

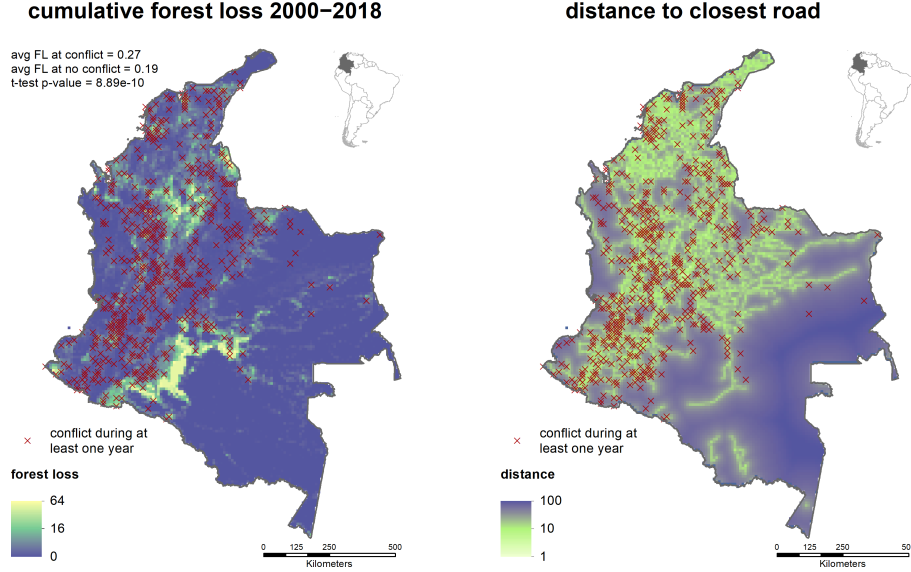


FIGURE 1. Temporally aggregated summary of the dataset described in Section 1.3. For visual purposes, the above color scales are square root- and \log_{10} -transformed, respectively. Conflicts are predictive of exceedances in forest loss (left), but this dependence is partly induced by a common dependence on transport infrastructure, which we measure by the mean distance to a road (right). Failing to account for this variable and other confounders biases our estimate of the causal influence of conflict on forest loss. Also, since both conflicts and forest loss exhibit complicated spatial dependence patterns, the independence assumptions underlying a standard two-sample t-test are likely to be violated. To correctly assess statements of statistical significance, we need a test which acknowledges the spatial dependence in the data.

papers report evidence that both positive and negative impacts of conflict on forest loss may happen in parallel, depending on the local conditions [e.g., Sánchez-Cuervo and Aide, 2013, Castro-Nunez et al., 2017]. Latest evidence suggests, however, that forest loss has increased substantially after the initiation of the peace process in protected areas [Armenteras et al., 2019, Clerici et al., 2020]. We believe that a purely data-driven approach can be a useful addition to this debate.

In our analysis, we use a spatio-temporal dataset containing measurements of the following variables.

- X_s^t : binary conflict indicator for location s at year t .
- Y_s^t : absolute forest loss in location s from year $t - 1$ to year t , measured in square kilometers.
- W_s^t : distance from location s to the closest road, measured in kilometers.

Data are annually aggregated, covering the years from 2000 to 2018, and spatially explicit at a $10\text{km} \times 10\text{km}$ -resolution. We provide a detailed description of the data processing in Section 4. A summary of the dataset can be seen in Figure 1. Visually, there is a strong positive dependence between the occurrence of a conflict and the loss of forest canopy. This observation is supported by simple summary statistics: the average forest loss across measurements classified as conflict events exceeds that from non-conflict events by almost 50%; a difference that is declared highly significant by a standard t-test (Figure 1, left). The strong significance of the statistical dependence between forest loss and conflict has been reported before [e.g., Landholm et al., 2019]. When seeking a causal explanation for the observed data, however, we regard such an analysis as flawed in two ways. First, both conflicts and forest loss predominantly occur in areas with good transport infrastructure (Figure 1, right), indicating that the potential causal effect of X on Y is confounded by W . In fact, we expect the existence of several other confounders (e.g., population density, market infrastructure, mining operations, cocaine plantations, etc.), many of which

may be unobserved. Failing to account for confounding variables leads to biased estimates of the causal effect. Second, strong spatial dependencies in X and Y reduce the effective sample size, and a standard t-test thus exaggerates the significance of the observed difference in sample averages. To test hypotheses about X and Y , we need statistical tests which are adapted to the spatio-temporal nature of data.

1.4 Contributions and structure of the paper

Apart from the case study, this paper contains three main theoretical contributions: the definition of a causal model for spatio-temporal data, a method for estimating causal effects, and a hypothesis test for the overall existence of such effects. Our class of causal models is introduced in Section 2. It translates the situation of a vector of covariates X that causally affect a real-valued response variable Y into a spatio-temporal setting. It allows for arbitrary influences of latent confounders, as long as these confounders do not vary across time. It further accommodates largely unspecified spatio-temporal dependence structures in the data. Within our model class, we conceptually define the causal effect of X and Y , propose an estimator of this quantity, and prove consistency. This finding is supported by a simulation study. In Section 3, we introduce a non-parametric hypothesis test for the overall existence of a causal effect, and prove that this test obtains valid level in finite samples. Section 4 applies our methodology to the above example. All data used for our analysis are publicly available. A description of how it can be obtained, along with an implementation of our method and reproducing scripts for all our figures and results, can be found at github.com/runesen/spatio_temporal_causality. All our proofs are contained in Appendix B.

2 Quantifying causal effects for spatio-temporal data

A spatio-temporal dataset may be viewed as a single realization of a spatio-temporal stochastic process, observed at discrete points in space and time. In this section, we provide a formal framework to quantify causal relationships among the components of a multivariate spatio-temporal process. This framework is presented in Section 2.1. In Section 2.2, we define the class of latent spatial confounder models (LSCMs) which will be the subject of study in this work, Section 2.3 shows how to estimate causal effects within this model class, and Section 2.4 discusses several extensions of our methodology.

2.1 Causal models for spatio-temporal processes

Throughout this section, let (Ω, \mathcal{A}, P) be some background probability space. A p -dimensional *spatio-temporal process* \mathbf{Z} is a random variable taking values in the sample space \mathcal{Z}_p of all $(\mathcal{B}(\mathbb{R}^2 \times \mathbb{N}), \mathcal{B}(\mathbb{R}^p))$ -measurable functions, where $\mathcal{B}(\cdot)$ denotes the Borel σ -algebra. We equip \mathcal{Z}_p with the σ -algebra \mathcal{F}_p , defined as the smallest σ -algebra such that for all $B \in \mathcal{B}(\mathbb{R}^p)$, the mapping $\mathcal{Z}_p \ni z \mapsto \int_B z(x)dx$ is $(\mathcal{F}_p, \mathcal{B}(\mathbb{R}))$ -measurable. The induced probability measure \mathbb{P} on the measurable space $(\mathcal{Z}_p, \mathcal{F}_p)$, for every $F \in \mathcal{F}_p$ defined by $\mathbb{P}(F) := P(\mathbf{Z}^{-1}(F))$, is said to be the *distribution of \mathbf{Z}* . Throughout this paper, we use the notation Z_s^t to denote the random vector obtained from marginalizing \mathbf{Z} at spatial location s and temporal instance t . We use \mathbf{Z}_s for the time series $(Z_s^t)_{t \in \mathbb{N}}$, \mathbf{Z}^t for the spatial process $(Z_s^t)_{s \in \mathbb{R}^2}$, and $\mathbf{Z}^{(S)}$ for the spatio-temporal process corresponding to the coordinates in $S \subseteq \{1, \dots, p\}$. We call a spatio-temporal process *weakly stationary* if the marginal distribution of Z_s^t is the same for all $(s, t) \in \mathbb{R}^2 \times \mathbb{N}$, and *time-invariant* if $\mathbb{P}(\mathbf{Z}^1 = \mathbf{Z}^2 = \dots) = 1$.

Multivariate spatio-temporal processes are used for the joint modeling of different phenomena, each of which corresponds to a coordinate process. Let us consider a decomposition of these coordinate processes into disjoint ‘bundles’. We are interested in specifying causal relations among these bundles while leaving the causal structure among variables within each bundle unspecified. Similarly to a graphical model [Lauritzen, 1996], our approach relies on a factorization of the joint distribution of \mathbf{Z} into a number of

components, each of which models the conditional distribution for one bundle given several others. This approach induces a graphical relation among the different bundles. We will equip these relations with a causal interpretation by additionally specifying the distribution of \mathbf{Z} under certain interventions on the data generating process. More formally, we have the following definition.

Definition 1 (Causal graphical models for spatio-temporal processes). *A causal graphical model for a p -dimensional spatio-temporal process \mathbf{Z} is a triplet $(\mathcal{S}, \mathcal{G}, \mathcal{P})$ consisting of*

- a family $\mathcal{S} = (S_j)_{j=1}^k$ of non-empty, disjoint sets $S_1, \dots, S_k \subseteq \{1, \dots, p\}$ with $\bigcup_{j=1}^k S_j = \{1, \dots, p\}$,
- a directed acyclic graph \mathcal{G} with vertices S_1, \dots, S_k , and
- a family $\mathcal{P} = (\mathcal{P}^j)_{j=1}^k$ of collections $\mathcal{P}^j = \{\mathbb{P}_z^j\}_{z \in \mathcal{Z}_{|\text{PA}_j|}}$ of distributions on $(\mathcal{Z}_{|S_j|}, \mathcal{F}_{|S_j|})$, where for every j , $\text{PA}_j := \bigcup_{i: S_i \rightarrow S_j \in \mathcal{G}} S_i$. Whenever $\text{PA}_j = \emptyset$, \mathcal{P}^j consists only of a single distribution which we denote by \mathbb{P}^j .

Since \mathcal{G} is acyclic, we can without loss of generality assume that S_1, \dots, S_k are indexed such that $S_i \not\rightarrow S_j$ in \mathcal{G} whenever $i > j$. The above components induce a unique joint distribution \mathbb{P} over \mathbf{Z} . For every $F = \times_{j=1}^k F_j$, it is defined by

$$\mathbb{P}(F) = \int_{F_1} \dots \int_{F_k} \mathbb{P}_{z^{(\text{PA}_k)}}^k(dz^{(S_k)}) \dots \mathbb{P}^1(dz^{(S_1)}). \quad (1)$$

We call \mathbb{P} the observational distribution. For each $j \in \{1, \dots, k\}$, the conditional distribution of $\mathbf{Z}^{(S_j)}$ given $\mathbf{Z}^{(\text{PA}_j)}$ as induced by \mathbb{P} equals \mathcal{P}^j . We define an intervention on $\mathbf{Z}^{(S_j)}$ as replacing \mathcal{P}^j by another model $\tilde{\mathcal{P}}^j$. This operation results in a new graphical model $(\mathcal{S}, \mathcal{G}, \tilde{\mathcal{P}})$ for \mathbf{Z} which induces, via (1), a new distribution $\tilde{\mathbb{P}}$, the interventional distribution.

Assume that we perform an intervention on $\mathbf{Z}^{(S_i)}$. By definition, the resulting interventional distribution differs from the observational distribution only in the way in which $\mathbf{Z}^{(S_i)}$ depends on $\mathbf{Z}^{(\text{PA}_i)}$, while all other conditional distributions $\mathbf{Z}^{(S_j)} | \mathbf{Z}^{(\text{PA}_j)}$, $j \neq i$, remain the same. This property is analogous to the modularity property of structural causal models [Haavelmo, 1944, Aldrich, 1989, Pearl, 2009, Peters et al., 2017] and justifies a causal interpretation of the conditionals in \mathcal{P} . We refer to the graph \mathcal{G} as the *causal structure* of \mathbf{Z} , and sometimes write $\mathbf{Z} = [\mathbf{Z}^{(S_k)} | \mathbf{Z}^{(\text{PA}_k)}] \dots [\mathbf{Z}^{(S_1)}]$ to emphasize this structure.

2.2 Latent spatial confounder model

Motivated by the example on conflict and forest loss introduced in Section 1.3, we are particularly interested in scenarios where a target variable Y is causally influenced by a vector of covariates X , and where (X, Y) are additionally affected by some latent variables H . In general, inferring causal effects under arbitrary influences of latent confounders is impossible, and we therefore need to impose additional restrictions on the variables in H . We here make the fundamental assumption that they do not vary across time (alternatively, one can assume that the hidden variables are invariant over space, see Section 2.4.3).

Definition 2 (Latent spatial confounder model). *Consider a spatio-temporal process $(\mathbf{X}, \mathbf{Y}, \mathbf{H}) = (X_s^t, Y_s^t, H_s^t)_{(s,t) \in \mathbb{R}^2 \times \mathbb{N}}$ over a real-valued response Y , a vector of covariates $X \in \mathbb{R}^d$ and a vector of latent variables $H \in \mathbb{R}^\ell$. We call a causal graphical model over $(\mathbf{X}, \mathbf{Y}, \mathbf{H})$ with causal structure $[\mathbf{Y} | \mathbf{X}, \mathbf{H}][\mathbf{X} | \mathbf{H}][\mathbf{H}]$ a latent spatial confounder model (LSCM) if both of the following conditions hold true for the observational distribution.*

- The latent process \mathbf{H} is weakly stationary and time-invariant.
- There exists a function $f : \mathbb{R}^{d+\ell+1} \rightarrow \mathbb{R}$ and an i.i.d. sequence $\varepsilon^1, \varepsilon^2, \dots$ of weakly-stationary spatial error processes, independent of (\mathbf{X}, \mathbf{H}) , such that

$$Y_s^t = f(X_s^t, H_s^t, \varepsilon_s^t) \quad \text{for all } (s, t) \in \mathbb{R}^2 \times \mathbb{N}. \quad (2)$$

Throughout this section, we assume that $(\mathbf{X}, \mathbf{Y}, \mathbf{H})$ come from an LSCM. The above definition says that for every s, t , Y_s^t depends on (\mathbf{X}, \mathbf{H}) only via (X_s^t, H_s^t) , and that this dependence remains the same for all points in space-time. Together with the weak stationarity of \mathbf{H} and ε , this assumption ensures that the average causal effect of X_s^t on Y_s^t (which we introduce below) remains the same for all s, t . Our model class imposes no restrictions on the marginal distribution of \mathbf{X} . The spatial dependence structure of the error process ε must have the same marginal distributions everywhere, but is otherwise unspecified (in particular, ε is not required to be stationary). The temporal independence assumption on ε is necessary for our construction of resampling tests, see Section 3. We now formally define our inferential target.

Definition 3 (Average causal effect). *The average causal effect of \mathbf{X} on \mathbf{Y} is defined as the function $f_{\text{AVE}(X \rightarrow Y)} : \mathbb{R}^d \rightarrow \mathbb{R}$, for every $x \in \mathbb{R}^d$ given by*

$$f_{\text{AVE}(X \rightarrow Y)}(x) := \mathbb{E}[f(x, H_0^1, \varepsilon_0^1)]. \quad (3)$$

Here, the causal effect is an average effect in that it takes the expectation over both the noise variable (as opposed to making counterfactual statements [Rubin, 1974]) and the hidden variables (see also Remark 6). The following proposition justifies $f_{\text{AVE}(X \rightarrow Y)}$ as a quantification of the causal influence of \mathbf{X} on \mathbf{Y} .

Proposition 4 (Causal interpretation). *Let $(s, t) \in \mathbb{R}^2 \times \mathbb{N}$ and $x \in \mathbb{R}^d$ be fixed, and consider any intervention on \mathbf{X} such that $X_s^t = x$ holds almost surely in the induced interventional distribution \mathbb{P}_x . We then have that*

$$\mathbb{E}_{\mathbb{P}_x}[Y_s^t] = f_{\text{AVE}(X \rightarrow Y)}(x),$$

i.e., $f_{\text{AVE}(X \rightarrow Y)}(x)$ is the expected value of Y_s^t under any intervention that enforces $X_s^t = x$.

In many practical applications, we do not have explicit knowledge of, or data from, the interventional distributions \mathbb{P}_x . If we have access to the causal graph, however, we can sometimes compute intervention effects from the observational distribution. In the i.i.d. setting, depending on which variables are observed, this can be done by covariate adjustment or G-computation [Pearl, 2009, Rubin, 1974, Shpitser et al., 2010], for example. The following proposition shows a similar result in the case of a latent spatial confounder model. It follows directly from Fubini's theorem.

Proposition 5 (Covariate adjustment). *Let $f_{Y|(X,H)}$ denote the regression function $(x, h) \mapsto \mathbb{E}[Y_s^t | X_s^t = x, H_s^t = h]$ (by definition of an LSCM, this function is the same for all s, t). For all $x \in \mathbb{R}^d$, it holds that*

$$f_{\text{AVE}(X \rightarrow Y)}(x) = \mathbb{E}[f_{Y|(X,H)}(x, H_0^1)]. \quad (4)$$

Proposition 5 shows that $f_{\text{AVE}(X \rightarrow Y)}$ is identified from the full observational distribution over $(\mathbf{X}, \mathbf{Y}, \mathbf{H})$ (given that the LSCM structure is known). Since \mathbf{H} is unobserved, the main challenge is to estimate (4) merely based on data from (\mathbf{X}, \mathbf{Y}) , see Section 2.3. (We discuss in Section 2.4.1 how to further include observable covariates that are allowed to vary over time.)

Remark 6 (An alternative definition of the average causal effect). *In our definition of the average causal effect (3), we take the expectation with respect to the hidden variables H . By the assumption of time-invariance, however, there is only a single replication of the spatial process \mathbf{H}^1 . One may argue that it is more relevant to define the inferential target in terms of that one realization, rather than in terms of a distribution over possible alternative outcomes which will never manifest themselves. This leads to the alternative definition of the average causal effect*

$$x \mapsto \lim_{S \rightarrow \infty} \frac{1}{(2S)^2} \int_{[-S, S]^2} \mathbb{E}[f(x, h_s^1, \varepsilon_0^1)] ds = \lim_{S \rightarrow \infty} \frac{1}{(2S)^2} \int_{[-S, S]^2} f_{Y|(X,H)}(x, h_s^1) ds,$$

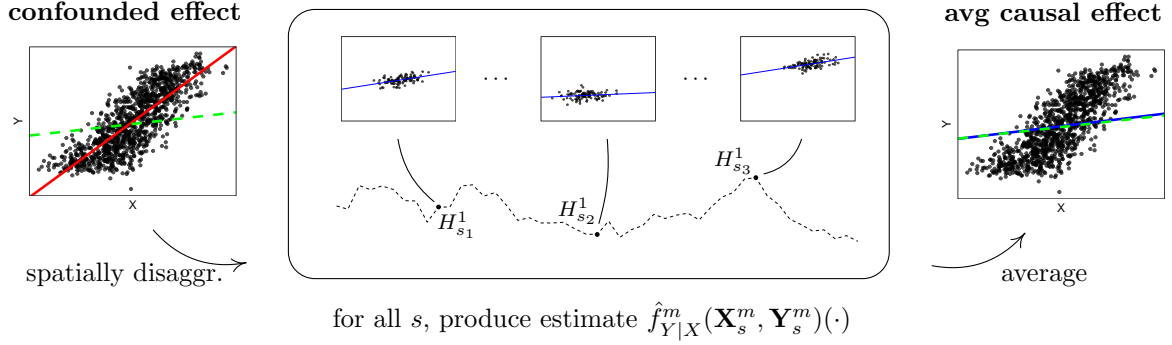


FIGURE 2. Conceptual idea for estimating the average causal effect (green dashed line) defined in (3). In both the left and right panel, we do not display the information of time and space. The figure in the middle shows the data at different locations $s \in \{s_1, \dots, s_n\}$, i.e., every small plot corresponds to a single time series. The dashed curve illustrates the unobserved realization of the spatial confounder H_s^t (for visual purposes, we here consider one-dimensional space). Due to this confounder, regressing Y_s^t on X_s^t (red line in left plot) leads to a biased estimator of the average causal effect. By exploiting the time-invariance of H_s^t , our estimator (blue line in right plot) removes this bias. This procedure is illustrated in the middle figure: at every location s , we observe several time instances (X_s^t, Y_s^t) , $t = 1, \dots, m$, with the same conditionals $Y_s^t | (X_s^t, H_s^t)$ and the same (unobserved) value of H_s^t . For each realization h_s of H_s^1 , we can therefore estimate the regression $f_{Y|(X,H)}(\cdot, h_s)$ only using the data $(\mathbf{X}_s^m, \mathbf{Y}_s^m)$ (blue lines in middle figure). A final estimate of the average causal effect (blue line in right plot) is obtained by approximating the expectation in (5) by a sample average over all spatial locations. We make this approach precise in Section 2.3.

assuming that the above limits exist. Under the assumption of ergodicity of \mathbf{H}^1 , the above expression coincides with Definition 3, but it is learnable from data, via the estimator introduced in Section 2.3, even if this is not the case.¹ Here, we choose the formulation in Definition 3 because we found that it results in a more comprehensible theory.

2.3 Estimation of the average causal effect

2.3.1 Definition and consistency

In practice, we only observe the process (\mathbf{X}, \mathbf{Y}) at a finite number of points in space and time. We assume that at every temporal instance, we observe the process at the same spatial locations $s_1, \dots, s_n \in \mathbb{R}^2$ (these locations need not lie on a regular grid). To simplify notation, we further assume that the observed time points are $t = 1, 2, \dots, m$, i.e., we have access to a dataset $(\mathbf{X}_n^m, \mathbf{Y}_n^m) = (X_s^t, Y_s^t)_{(s,t) \in \{s_1, \dots, s_n\} \times \{1, \dots, m\}}$. The proposed method is based on the following key idea: for every $s \in \{s_1, \dots, s_n\}$, we observe several time instances (X_s^t, Y_s^t) , $t \in \{1, \dots, m\}$, all with the same conditionals $Y_s^t | (X_s^t, H_s^t)$. Since \mathbf{H} is time-invariant, we can, for every s , estimate $f_{Y|(X,H)}(\cdot, h_s)$ for the (unobserved) realization h_s of H_s^1 using the data (X_s^t, Y_s^t) , $t \in \{1, \dots, m\}$. The expectation in (4) is then approximated by averaging estimates obtained from different spatial locations. This idea is visualized in Figure 2. More formally, our method requires as input a model class for the regressions $f_{Y|(X,H)}(\cdot, h)$, $h \in \mathbb{R}^\ell$, alongside with a suitable estimator $\hat{f}_{Y|X} = (\hat{f}_{Y|X}^m)_{m \in \mathbb{N}}$, and returns

$$\hat{f}_{\text{AVE}(X \rightarrow Y)}^{nm}(\mathbf{X}_n^m, \mathbf{Y}_n^m)(x) := \frac{1}{n} \sum_{i=1}^n \hat{f}_{Y|X}^m(\mathbf{X}_{s_i}^m, \mathbf{Y}_{s_i}^m)(x), \quad (5)$$

¹We are grateful to Steffen Lauritzen for emphasizing this viewpoint.

an estimator of the average causal effect (3) within the given model class. In Section 3, we further provide a statistical test for the overall existence of a causal effect. Our approach may be seen as summarizing the output of a spatially varying regression model [e.g., Gelfand et al., 2003] that is allowed to change arbitrarily from one location to the other (within the model class dictated by $\hat{f}_{Y|X}$). By permitting such flexibility, our method does not rely on observing data from a continuous or spatially connected domain, and accommodates complex influences of the latent variables. An implementation can be found in our code package, see Section 1.4.

To prove consistency of our estimator, we let the number of observable points in space-time increase. Let therefore $(s_n)_{n \in \mathbb{N}} \subseteq \mathbb{R}^2$ be a sequence of spatial coordinates, and consider the array of data $(\mathbf{X}_n^m, \mathbf{Y}_n^m)_{n,m \geq 1}$, where for every $n, m \in \mathbb{N}$, $(\mathbf{X}_n^m, \mathbf{Y}_n^m) = (X_s^t, Y_s^t)_{(s,t) \in \{s_1, \dots, s_n\} \times \{1, \dots, m\}}$. We want to prove that the corresponding sequence of estimators (5) consistently estimates (3). To obtain such a result, we need two central assumptions.

Assumption A1 (Law of Large Numbers for the latent process). *For all measurable functions $\varphi : \mathbb{R}^\ell \rightarrow \mathbb{R}$ with $\mathbb{E}[|\varphi(H_0^1)|] < \infty$ it holds that $\frac{1}{n} \sum_{i=1}^n \varphi(H_{s_i}^1) \rightarrow \mathbb{E}[\varphi(H_0^1)]$ in probability as $n \rightarrow \infty$.*

The above assumption ensures that, for an increasing number of spatial locations at which data are observed, the spatial average in (5) approximates the expectation in (3). As the number of observed time points tends to infinity, we require the estimators $\hat{f}_{Y|X}^m$ to converge to the integrand in (3), at least in some area $\mathcal{X} \subseteq \mathbb{R}^d$.

Assumption A2 (Consistent estimators of the conditional expectations). *There exists $\mathcal{X} \subseteq \mathbb{R}^d$ s.t. for all $x \in \mathcal{X}$ and $s \in \mathbb{R}^2$, it holds that $\hat{f}_{Y|X}^m(\mathbf{X}_s^m, \mathbf{Y}_s^m)(x) - f_{Y|(X,H)}(x, H_s^1) \rightarrow 0$ in probability as $m \rightarrow \infty$.*

A slightly stronger, but maybe more intuitive formulation is to require the above consistency to hold conditionally on \mathbf{H} , i.e., assuming that for all $x \in \mathcal{X}$, $s \in \mathbb{R}^2$ and almost all \mathbf{h} , $\hat{f}_{Y|X}^m(\mathbf{X}_s^m, \mathbf{Y}_s^m)(x) \rightarrow f_{Y|(X,H)}(x, h_s^1)$ as $m \rightarrow \infty$, in probability under $\mathbb{P}(\cdot | \mathbf{H} = \mathbf{h})$. It follows from the dominated convergence theorem that this assumption implies Assumption A2.

Under Assumptions A1 and A2, we obtain the following consistency result.

Theorem 7 (Consistent estimator of the average causal effect). *Let $(\mathbf{X}, \mathbf{Y}, \mathbf{H})$ come from an LSCM as defined in Definition 2. Let $(s_n)_{n \in \mathbb{N}}$ be a sequence of spatial coordinates such that the marginalized process $(H_{s_n}^1)_{n \in \mathbb{N}}$ satisfies Assumption A1, and assume that for all $x \in \mathcal{X}$, $\mathbb{E}[|f_{Y|(X,H)}(x, H_0^1)|] < \infty$. Let furthermore $\hat{f}_{Y|X} = (\hat{f}_{Y|X}^m)_{m \in \mathbb{N}}$ be an estimator satisfying Assumption A2. We then have the following consistency result. For all $x \in \mathcal{X}$, $\delta > 0$ and $\alpha > 0$, there exists $N \in \mathbb{N}$ such that for all $n \geq N$ we can find $M_n \in \mathbb{N}$ such that for all $m \geq M_n$ we have that*

$$\mathbb{P}\left(\left|\hat{f}_{\text{AVE}(X \rightarrow Y)}^{nm}(\mathbf{X}_n^m, \mathbf{Y}_n^m)(x) - f_{\text{AVE}(X \rightarrow Y)}(x)\right| > \delta\right) \leq \alpha. \quad (6)$$

Apart from the LSCM structure, the above result does not rely on any particular distributional properties of the data. Assumptions A1 and A2 do not impose strong restrictions on the data generating process and hold true for several model classes, including linear and nonlinear models. Below, we provide sufficient conditions under which these assumptions are true.

2.3.2 Sufficient conditions for Assumptions A1 and A2

For Assumption A1, we consider a stationary Gaussian setup. By considering a regular spatial sampling scheme, we can make use of standard ergodic theorems for stationary and ergodic time series.

Proposition 8 (Sufficient conditions for Assumption A1). *Assume that \mathbf{H}^1 is a stationary multivariate Gaussian process with covariance function $C : \mathbb{R}^2 \rightarrow \mathbb{R}^{\ell \times \ell}$, i.e., $C(h) = \text{Cov}(H_s^1, H_{s+h}^1)$ for all $s, h \in \mathbb{R}^2$. Assume that $C(h) \rightarrow 0$ entrywise as $\|h\|_2 \rightarrow \infty$. Consider a regular grid $\{s_1^1, s_2^1, \dots\} \times \{s_1^2, s_2^2, \dots, s_m^2\} \subseteq \mathbb{R}^2$, where $s_1^1 < s_2^1 < \dots$ are equally spaced, and let $(s_n)_{n \in \mathbb{N}}$ be the spatial sampling scheme for every $i \in \mathbb{N}$ and $j \in \{1, \dots, m\}$ given as $s_{(i-1)m+j} = (s_i^1, s_j^2)$. Then, the process $(H_{s_n}^1)_{n \in \mathbb{N}}$ satisfies Assumption A1.*

For Assumption A2, we consider the slightly stronger version formulated conditionally on \mathbf{H} . We let $\mathcal{H} \subseteq \mathcal{Z}_\ell$ denote the set of all functions $\mathbf{h} : \mathbb{R}^2 \times \mathbb{N} \rightarrow \mathbb{R}^\ell$ that are constant in the time-argument. Since \mathbf{H} is time-invariant, we have that $\mathbb{P}(\mathbf{H} \in \mathcal{H}) = 1$, and it therefore suffices to prove the statement for all $\mathbf{h} \in \mathcal{H}$. Below, we use, for every $\mathbf{h} \in \mathcal{H}$, $\mathbb{P}_{\mathbf{h}}$ to denote the conditional distribution $\mathbb{P}(\cdot | \mathbf{H} = \mathbf{h})$ and $\mathbb{E}_{\mathbf{h}}$ for the expectation with respect to $\mathbb{P}_{\mathbf{h}}$.

We now make some structural assumptions on the function f in (2), which allow us to parametrically estimate the regressions $x \mapsto f_{Y|(X,H)}(x, h)$. Let $\{\varphi_1, \dots, \varphi_p\}$ be a known basis of continuous functions on \mathbb{R}^d , and with $\varphi_1 \equiv 1$ an intercept term. With $\varphi := (\varphi_1, \dots, \varphi_p)$, we make the following assumptions on the underlying LSCM.

(L1) There exist functions $f_1 : \mathbb{R}^\ell \rightarrow \mathbb{R}^p$ and $f_2 : \mathbb{R}^{\ell+1} \rightarrow \mathbb{R}$ such that Equation (2) splits into

$$Y_s^t = \varphi(X_s^t)^\top f_1(H_s^t) + f_2(H_s^t, \varepsilon_s^t) \quad \text{for all } (s, t) \in \mathbb{R}^2 \times \mathbb{N},$$

and such that for all $h \in \mathbb{R}^\ell$, $f_2(h, \varepsilon_0^1)$ has finite second moment.

For every s, t , define $\xi_s^t = f_2(H_s^t, \varepsilon_s^t)$. We can w.l.o.g. assume that for all s, t and h , $\mathbb{E}[\xi_s^t | H_s^t = h] = 0$. (Since $\varphi_1 \equiv 1$, this can always be accommodated by adding $h \mapsto \mathbb{E}[\xi_s^t | H_s^t = h]$ to the first coordinate of f_1 .) For every fixed $\mathbf{h} \in \mathcal{H}$ and $s \in \mathbb{R}^2$, assumption (L1) says that, under $\mathbb{P}_{\mathbf{h}}$, $(\mathbf{X}_s, \mathbf{Y}_s)$ follows a simple regression model, where $\mathbb{E}[Y_s^t | X_s^t]$ depends linearly on $\varphi(X_s^t)$. For arbitrary but fixed h_s^1 , we can therefore estimate $x \mapsto \mathbb{E}[Y_s^1 | X_s^1 = x, H_s^1 = h_s^1]$ using standard OLS estimation. For every $s \in \mathbb{R}^2$ and $m \in \mathbb{N}$, let $\Phi_s^m \in \mathbb{R}^{m \times p}$ be the design matrix given by $(\Phi_s^m)_{ij} = \varphi_j(X_s^i)$. We define an estimator $\hat{f}_{Y|X}^m = (\hat{f}_{Y|X}^m)_{m \in \mathbb{N}}$, for every $x \in \mathbb{R}^d$ and $m \in \mathbb{N}$ by

$$\hat{f}_{Y|X}^m(\mathbf{X}_s^m, \mathbf{Y}_s^m)(x) = \varphi(x)^\top \hat{\gamma}_s^m, \quad (7)$$

where $\hat{\gamma}_s^m := ((\Phi_s^m)^\top \Phi_s^m)^{-1} (\Phi_s^m)^\top \mathbf{Y}_s^m$. To formally prove consistency of (7), we need some regularity conditions on the predictors \mathbf{X} .

(L2) For all $\mathbf{h} \in \mathcal{H}$, $s \in \mathbb{R}^2$ and $\delta > 0$, it holds that

$$\lim_{m \rightarrow \infty} \mathbb{P}_{\mathbf{h}}(\|\frac{1}{m} (\Phi_s^m)^\top \xi_s^m\|_2 > \delta) = 0.$$

(L3) For all $\mathbf{h} \in \mathcal{H}$, $s \in \mathbb{R}^2$, there exists $c > 0$ such that

$$\lim_{m \rightarrow \infty} \mathbb{P}_{\mathbf{h}}(\lambda_{\min}(\frac{1}{m} (\Phi_s^m)^\top \Phi_s^m) \leq c) = 0,$$

where λ_{\min} denotes the minimal eigenvalue.

We first state the result and discuss assumptions (L2) and (L3) afterwards.

Proposition 9 (Sufficient conditions for Assumption A2). *Assume that $(\mathbf{X}, \mathbf{Y}, \mathbf{H})$ come from an LSCM satisfying (L1)–(L3). Then, Assumption A2 is satisfied with $\mathcal{X} = \mathbb{R}^d$ and with $\hat{f}_{Y|X}^m$ as defined in (7).*

Since for every $(s, t) \in \mathbb{R}^2 \times \mathbb{N}$ and $\mathbf{h} \in \mathcal{H}$, X_s^t and ξ_s^t are independent under $\mathbb{P}_{\mathbf{h}}$ with $\mathbb{E}_{\mathbf{h}}[\xi_s^t] = 0$, (L2) states a natural LLN-type condition, which is satisfied under suitable constraints on the temporal dependence structure in \mathbf{X} , and on its variance. Assumption (L3) says that, with probability tending to one, the matrix $\frac{1}{m} (\Phi_s^m)^\top \Phi_s^m$ is bounded away from singularity as $m \rightarrow \infty$. This is in particular satisfied if $\frac{1}{m} (\Phi_s^m)^\top \Phi_s^m$ converges in probability entrywise to some matrix which is strictly positive definite. In Appendix A, we give two examples in which this is the case.

2.3.3 An example LSCM

To illustrate the consistency result in Theorem 7, we now consider a simple example with one covariate ($d = 1$) and two hidden variables ($\ell = 2$).

Example 10 (Latent Gaussian process and a linear average causal effect). *Let $\zeta, \psi, \xi^t, \varepsilon^t$, $t \in \mathbb{N}$, be independent versions of a univariate stationary spatial Gaussian process with mean 0 and covariance function $u \mapsto e^{-\frac{1}{2}\|u\|_2}$. For notational simplicity, let $\bar{\mathbf{H}}$ and $\tilde{\mathbf{H}}$ denote the respective first and second coordinate process of \mathbf{H} . We define a marginal distribution over \mathbf{H} and conditional distributions $\mathbf{X} | \mathbf{H}$ and $\mathbf{Y} | (\mathbf{X}, \mathbf{H})$ by specifying that for all $(s, t) \in \mathbb{R}^2 \times \mathbb{N}$,*

$$\begin{aligned} H_s^t &= (\bar{H}_s^t, \tilde{H}_s^t) = (\zeta_s, 1 + \frac{1}{2}\zeta_s + \frac{\sqrt{3}}{2}\psi_s), \\ X_s^t &= \exp(-\|s\|_2^2/1000) + (0.2 + 0.1 \cdot \sin(2\pi t/100)) \cdot \bar{H}_s^t \cdot \tilde{H}_s^t + 0.5 \cdot \xi_s^t, \\ Y_s^t &= (1.5 + \bar{H}_s^t \cdot \tilde{H}_s^t) \cdot X_s^t + (\bar{H}_s^t)^2 + |\tilde{H}_s^t| \cdot \varepsilon_s^t. \end{aligned}$$

Interventions on \mathbf{X} , \mathbf{Y} or \mathbf{H} are defined as in Definition 1. In this LSCM, the average causal effect $f_{\text{AVE}(X \rightarrow Y)}$ is the linear function $x \mapsto \beta_0 + \beta_1 x$, with $\beta_0 := \mathbb{E}[(\bar{H}_0^1)^2] = 1$ and $\beta_1 := 1.5 + \mathbb{E}[\bar{H}_0^1 \cdot \tilde{H}_0^1] = 2$. We define a spatial sampling scheme $(s_i)_{i \in \mathbb{N}}$ for every $j \in \mathbb{N}$ and $k \in \{1, \dots, 25\}$ by $s_{25 \cdot (j-1) + k} = (j, k)$. Given a sample $(\mathbf{X}_n^m, \mathbf{Y}_n^m) = (X_s^t, Y_s^t)_{(s,t) \in \{s_1, \dots, s_n\} \times \{1, \dots, m\}}$ from (\mathbf{X}, \mathbf{Y}) , we construct an estimator of $f_{\text{AVE}(X \rightarrow Y)}$ by

$$\hat{f}_{\text{AVE}(X \rightarrow Y)}^{nm}(\mathbf{X}_n^m, \mathbf{Y}_n^m)(x) = \frac{1}{n} \sum_{i=1}^n (1 \ x) \hat{\beta}_{\text{OLS}}^m(\mathbf{X}_{s_i}^m, \mathbf{Y}_{s_i}^m), \quad (8)$$

where $\hat{\beta}_{\text{OLS}}^m(\mathbf{X}_{s_i}^m, \mathbf{Y}_{s_i}^m) \in \mathbb{R}^2$ is the OLS estimator for the linear regression at spatial location s_i , that is of $\mathbf{Y}_{s_i}^m = (Y_{s_i}^1, \dots, Y_{s_i}^m)$ on $\mathbf{X}_{s_i}^m = (X_{s_i}^1, \dots, X_{s_i}^m)$ (we assume that the regression includes an intercept term). It follows by Propositions 8 and 9 (see in particular Example 14 and Remark 16 in Appendix A) that Assumptions A1 and A2 are satisfied.² Hence, (8) is a consistent estimator of $f_{\text{AVE}(X \rightarrow Y)}$.

Figure 3 shows results from a numerical experiment based on Example 10. The left panel shows the simulated dataset, the plot in the middle represents our method, and the right panel illustrates that the estimator is consistent. More details are provided in the figure caption. The example shows that we can estimate causal effects even under complex influences of the latent process \mathbf{H} . To construct the estimator $\hat{f}_{\text{AVE}(X \rightarrow Y)}^{nm}$, we have used that the influence of (\mathbf{X}, \mathbf{H}) on \mathbf{Y} is linear in \mathbf{X} . It is worth noting, however, that we do not assume knowledge of the particular functional dependence of \mathbf{Y} on \mathbf{H} ; we obtain consistency under any influence of the form $Y_s^t = f_1(H_s^t) \cdot X_s^t + f_2(H_s^t, \varepsilon_s^t)$, see Proposition 9.

2.4 Extensions

2.4.1 Observed confounders

For simplicity, we have until now assumed that the only confounders of (X, Y) are the variables in H . Our method naturally extends to settings with observed (time- and space-varying) confounders. Let $W \in \mathbb{R}^p$ be a vector of observed covariates, and consider a causal graphical model over $(\mathbf{X}, \mathbf{W}, \mathbf{Y}, \mathbf{H})$ with causal structure $[\mathbf{Y} | \mathbf{X}, \mathbf{W}, \mathbf{H}][\mathbf{X} | \mathbf{W}, \mathbf{H}][\mathbf{W}, \mathbf{H}]$. Similarly to Definition 2, assume that \mathbf{W} and \mathbf{H} are weakly stationary, \mathbf{H} is time-invariant, and there exists a function $f : \mathbb{R}^{d+p+\ell+1} \rightarrow \mathbb{R}$ and an i.i.d. sequence $\varepsilon^1, \varepsilon^2, \dots$ of weakly stationary error processes, independent of $(\mathbf{X}, \mathbf{W}, \mathbf{H})$, such that

$$Y_s^t = f(X_s^t, W_s^t, H_s^t, \varepsilon_s^t) \quad \text{for all } (s, t) \in \mathbb{R}^2 \times \mathbb{N}. \quad (9)$$

²Strictly speaking, Example 14 and Remark 16 show that (L1)–(L3) are satisfied for bounded basis functions. We are confident that the same holds true in the current example.

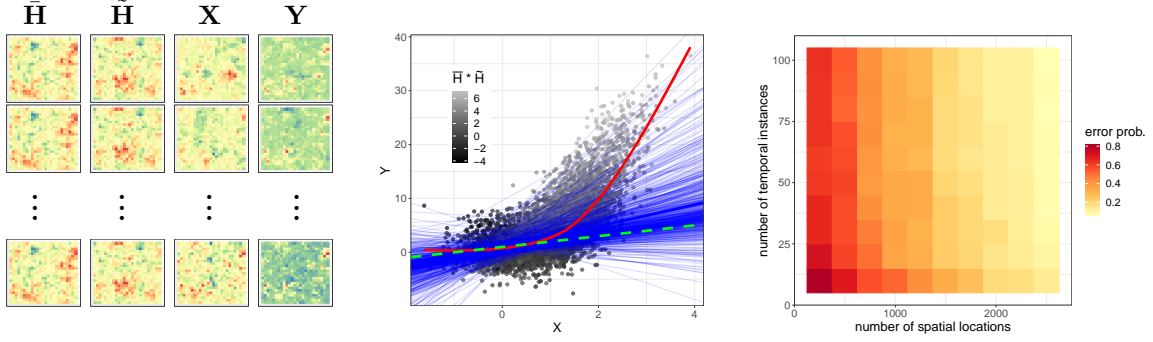


FIGURE 3. Results for applying our methodology to the LSCM in Example 10. The left panel shows a sample dataset of the process $(\mathbf{X}, \mathbf{Y}, \mathbf{H})$ observed at the spatial grid $\{1, \dots, 25\} \times \{1, \dots, 25\} \subseteq \mathbb{R}^2$ and at several temporal instances. For the sake of illustration, each square has its own colorscale, and colors are therefore not comparable across plots. The middle panel illustrates the output from our method applied to the same dataset. The average causal effect, our inferential target, is indicated by a dashed green line. Due to confounding by \mathbf{H} , a standard nonlinear regression (red curve) severely overestimates the causal influence of \mathbf{X} on \mathbf{Y} . By estimating the dependence between \mathbf{X} and \mathbf{Y} in each spatial location separately (thin blue lines), and aggregating the results into a final estimate (thick blue line), all spatial confounding is removed. In the right panel, we investigate the consistency result from Theorem 7 empirically. For increasing numbers of spatial locations n (shown on the x -axis) and temporal instances m (shown on the y -axis), we generate several datasets $(\mathbf{X}_{n,i}^m, \mathbf{Y}_{n,i}^m)$, $i = 1, \dots, 100$, compute estimates $\hat{\beta}_i^{nm}$ of the causal coefficients β , and use these to compute empirical error probabilities $\hat{\mathbb{P}}(\|\hat{\beta}^{nm} - \beta\|_2 > \delta)$. In the above plot, we have chosen $\delta = 0.2$. As n and m increase, the error probability tends towards zero.

We define the average causal effect of \mathbf{X} on \mathbf{Y} , for every $x \in \mathbb{R}^d$, by

$$f_{\text{AVE}(X \rightarrow Y)}(x) = \mathbb{E}[f(x, W_0^1, H_0^1, \varepsilon_0^1)].$$

It is straight-forward to show that this function enjoys the same causal interpretation as given in Proposition 4. Similarly to Proposition 5, we have that for all $x \in \mathbb{R}^d$, it holds that

$$f_{\text{AVE}(X \rightarrow Y)}(x) = \mathbb{E}[f_{Y|(X,W,H)}(x, W_0^1, H_0^1)],$$

where $f_{Y|(X,W,H)}$ is the regression function of Y_s^t onto (X_s^t, W_s^t, H_s^t) . As an estimator for the case where \mathbf{H} remains unobserved, we then use

$$\hat{f}_{\text{AVE}(X \rightarrow Y)}^{nm}(\mathbf{X}_n^m, \mathbf{Y}_n^m, \mathbf{W}_n^m)(x) := \frac{1}{n} \sum_{i=1}^n \hat{\mathbb{E}}_W[f_{Y|(X,W)}^m(\mathbf{X}_{s_i}^m, \mathbf{Y}_{s_i}^m, \mathbf{W}_{s_i}^m)(x, W_0^1)],$$

where $\hat{\mathbb{E}}_W$ is the expectation w.r.t. some estimate of the marginal distribution of W .

2.4.2 Temporally lagged causal effects

We can incorporate temporally lagged causal effects by allowing the function f in (2) to depend on past values of the predictors. That is, we model a joint causal influence of the past $k \geq 1$ temporal instances of the predictors by assuming the existence of a function $f : \mathbb{R}^{d \cdot k + \ell + 1} \rightarrow \mathbb{R}$ and an i.i.d. sequence $\varepsilon^1, \varepsilon^2, \dots$ such that

$$Y_s^t = f(X_s^{t-k+1}, \dots, X_s^t, H_s^t, \varepsilon_s^t) \quad \text{for all } s \in \mathbb{R}^2 \text{ and } t \geq k.$$

In this case, the average causal effect (3) is a function $\mathbb{R}^{d \cdot k} \rightarrow \mathbb{R}$ which can be estimated, similarly to (5), using a regression estimator $\hat{f}_{Y|X}^m$ of Y_s^t onto $(X_s^{t-k+1}, \dots, X_s^t)$.

2.4.3 Exchanging the role of space and time

We have assumed that the hidden confounders do not vary across time. This assumption allowed us to estimate the regression $x \mapsto \mathbb{E}[Y_s^t | X_s^t = x, H_s^t = h]$ at all unobserved values h . In fact, our method can be formulated in more general terms. If $(\mathbf{X}, \mathbf{Y}, \mathbf{H})$ is a multivariate process defined on some general, possibly random, index set $\mathcal{I} = I_1 \times \dots \times I_p$ (see the definition of a data cube [Mahecha et al., 2020]), it is enough to require \mathbf{H} to be invariant across one (or several) of the dimensions in \mathcal{I} . Similarly to (5), the idea is then to estimate the dependence of \mathbf{Y} on (\mathbf{X}, \mathbf{H}) along these invariant dimensions, followed by an aggregation across the remaining dimensions. In case of a spatio-temporal process, for example, our method also applies if the hidden variables are constant across space, rather than time.

3 Testing for the existence of causal effects

The previous section has been concerned with the quantification and estimation of the causal effect of X on Y . In this section, we introduce hypothesis tests for this effect being non-zero. We consider the null hypothesis

$$H_0 : (\mathbf{X}, \mathbf{Y}) \text{ come from an LSCM with a function } f \text{ that is constant w.r.t. } X_s^t,$$

which formalizes the assumption of “no causal influence of X on Y ” within the framework of LSCMs. We construct a non-parametric hypothesis test for H_0 using data resampling. Our approach acknowledges the existence of spatial dependence in the data without modeling it explicitly. It thus does not rely on distributional assumptions apart from the LSCM structure.

For the construction of a resampling test, we closely follow the setup presented in Pfister et al. [2018]. We require a data permutation scheme which, under the null hypothesis, leaves the distribution of the data unaffected. In particular, it must preserve the dependence between \mathbf{X} and \mathbf{Y} that is induced by \mathbf{H} . The idea is to permute observations of \mathbf{Y} corresponding to the same (unobserved) values of \mathbf{H} . Since \mathbf{H} is assumed to be constant within every spatial location, this is achieved by permuting \mathbf{Y} along the time axis. Let $(\mathbf{X}_n^m, \mathbf{Y}_n^m)$ be the observed data. For every $(\mathbf{x}, \mathbf{y}) \in \mathbb{R}^{(d+1) \times n \times m}$ and every permutation σ of the elements in $\{1, \dots, m\}$, let $\sigma(\mathbf{x}, \mathbf{y}) \in \mathbb{R}^{(d+1) \times n \times m}$ denote the permuted array with entries $(\sigma(x, y))_s^t = (x_s^t, y_s^{\sigma(t)})$. We then have the following exchangeability property.

Proposition 11 (Exchangeability). *For any permutation σ of the elements in $\{1, \dots, m\}$, we have that, under H_0 ,*

$$\sigma(\mathbf{X}_n^m, \mathbf{Y}_n^m) \text{ is equal in distribution to } (\mathbf{X}_n^m, \mathbf{Y}_n^m).$$

Proposition 11 is the cornerstone for the construction of a valid resampling test. Under the null hypothesis, we can compute pseudo-replications of the observed sample $(\mathbf{X}_n^m, \mathbf{Y}_n^m)$ using the permutation scheme described above. Given any test statistic $\hat{T} : \mathbb{R}^{(d+1) \times n \times m} \rightarrow \mathbb{R}$, we obtain a p -value for H_0 by comparing the value of \hat{T} calculated on the original dataset with the empirical null distribution of \hat{T} obtained from the resampled datasets. The choice of \hat{T} determines the power of the test. More formally, let $M := m!$ and let $\sigma_1, \dots, \sigma_M$ be all permutations of the elements in $\{1, \dots, m\}$. By Proposition 11, each of these permutations yields a new dataset with the same distribution as $(\mathbf{X}_n^m, \mathbf{Y}_n^m)$. Let $B \in \mathbb{N}$ and let k_1, \dots, k_B be independent, uniform draws from $\{1, \dots, M\}$. For every (\mathbf{x}, \mathbf{y}) , we define

$$p_{\hat{T}}(\mathbf{x}, \mathbf{y}) := \frac{1 + |\{b \in \{1, \dots, B\} : \hat{T}(\sigma_{k_b}(\mathbf{x}, \mathbf{y})) \geq \hat{T}(\mathbf{x}, \mathbf{y})\}|}{1 + B},$$

and construct for every $\alpha \in (0, 1)$ a test $\varphi_{\hat{T}}^\alpha : \mathbb{R}^{(d+1) \times n \times m} \rightarrow \{0, 1\}$ of H_0 defined by $\varphi_{\hat{T}}^\alpha = 1 \Leftrightarrow p_{\hat{T}} \leq \alpha$.³ The following level guarantee for $\varphi_{\hat{T}}^\alpha$ follows directly from [Pfister et al., 2018, Proposition B.4].

³Two-sided tests can be obtained using $p_{\hat{T}, 2\text{-sided}} := \min(1, 2 \cdot \min(p_{\hat{T}}, p_{-\hat{T}}))$, for example.

Corollary 12 (Level guarantee of resampling test). *Assume that for all $k, \ell \in \{1, \dots, B\}$, $k \neq \ell$, it holds that, under H_0 ,*

$$\mathbb{P}(\hat{T}(\sigma_k(\mathbf{X}_n^m, \mathbf{Y}_n^m)) = \hat{T}(\sigma_\ell(\mathbf{X}_n^m, \mathbf{Y}_n^m))) = 0.$$

Then, for every $\alpha \in (0, 1)$, the test $\varphi_{\hat{T}}^\alpha$ has correct level α .

Corollary 12 ensures valid test level for a large class of test statistics. The particular choice of test statistic should depend on the alternative hypothesis that we seek to have power against. Within the LSCM model class, it makes sense to quantify deviations from the null hypothesis using functionals of the average causal effect, i.e., $T = \psi(f_{\text{AVE}(X \rightarrow Y)})$ for some suitable function ψ . As a test statistic, we then use the plug-in estimator

$$\hat{T}(\mathbf{X}_n^m, \mathbf{Y}_n^m) = \psi(\hat{f}_{\text{AVE}(X \rightarrow Y)}^{nm}(\mathbf{X}_n^m, \mathbf{Y}_n^m)).$$

An implementation of the above testing procedure is contained in our code package, see Section 1.4.

4 Conflict and forest loss in Colombia

We now return to the problem of conflict (\mathbf{X}) and forest loss (\mathbf{Y}) introduced in Section 1.3. We first describe our data sources in Section 4.1, and then apply our proposed methodology in Section 4.2. In Section 4.3, we introduce two alternative approaches for comparison, Section 4.4 contains our results, and Section 4.5 interprets these results in light of the Colombian peace process.

4.1 Data description and preprocessing

Our analysis is based on two main datasets: (1) a remote sensing-based forest loss dataset for the period 2000–2018, which identifies annual forest loss at a spatial resolution of $30\text{m} \times 30\text{m}$ using Landsat satellites [Hansen et al., 2013]. Here, forest loss is defined as complete canopy removal. (2) Spatially explicit information on conflict events from 2000 to 2018, based on the Georeferenced Event Dataset (GED) from the Uppsala Conflict Data Program (UCDP) [Croicu and Sundberg, 2015]. In this dataset, a conflict event is defined as “an incident where armed force was used by an organized actor against another organized actor, or against civilians, resulting in at least one direct death at a specific location and a specific date” [Sundberg and Melander, 2013]. Such events were identified through global newswire reporting, global monitoring of local news, and other secondary sources such as reports by non-governmental organizations (for information on the data collection as well as control for quality and consistency of the data, please refer to Sundberg and Melander [2013] and Croicu and Sundberg [2015]). We homogenized these datasets through aggregation to a spatial resolution of $10\text{km} \times 10\text{km}$ by averaging the annual forest loss within each grid, and by counting all conflict events occurring in the same year and within the same grid. As a proxy for local transport infrastructure, we additionally calculated, for each spatial grid, the average Euclidean distance to the closest road segment, using spatial data from <https://diva-gis.org> containing all primary and secondary roads in Colombia. We regard this variable as relatively constant throughout the considered time-span.

4.2 Quantifying the causal influence of conflict on forest loss

We assume that (\mathbf{X}, \mathbf{Y}) come from an LSCM as defined in Definition 2. Since X_s^t is binary, we can characterize the causal influence of \mathbf{X} on \mathbf{Y} by $T := f_{\text{AVE}(X \rightarrow Y)}(1) - f_{\text{AVE}(X \rightarrow Y)}(0)$, i.e., the difference in expected forest loss $\mathbb{E}[Y_s^t]$ under the respective interventions enforcing conflict ($X_s^t := 1$) and peace ($X_s^t := 0$). Positive values of T correspond to an augmenting effect of conflict on forest loss and negative values correspond to a reducing effect. Our goal is to estimate T , and to test the hypothesis $H_0 : T = 0$ (no causal effect of \mathbf{X} on \mathbf{Y}). To construct an estimator of the average causal effect of the form (5), we

require estimators of the conditional expectations $x \mapsto f_{Y|(X,H)}(x, h)$. Since X_s^t is binary, we use simple sample averages of the response variable. To make the resulting estimator of $f_{\text{AVE}(X \rightarrow Y)}$ well-defined, we omit all locations which do not contain at least one observation from each of the regimes $X_s^t = 0$ and $X_s^t = 1$. More precisely, let $(\mathbf{X}_n^m, \mathbf{Y}_n^m)$ be the observed dataset. We then use the estimator

$$\hat{f}_{\text{AVE}(X \rightarrow Y)}^{nm}(\mathbf{X}_n^m, \mathbf{Y}_n^m)(x) = \frac{1}{|\mathcal{I}_n^m|} \sum_{i \in \mathcal{I}_n^m} \frac{1}{|\{t : X_{s_i}^t = x\}|} \sum_{t: X_{s_i}^t = x} Y_{s_i}^t, \quad x \in \{0, 1\}, \quad (10)$$

where $\mathcal{I}_n^m := \{i \in \{1, \dots, n\} : \text{there exist } t_0, t_1 \in \{1, \dots, m\} \text{ s.t. } X_{s_i}^{t_0} = 0 \text{ and } X_{s_i}^{t_1} = 1\}$. To test H_0 , we use the resampling test introduced in Section 3 with test statistic $\hat{T} = \hat{f}_{\text{AVE}(X \rightarrow Y)}^{nm}(1) - \hat{f}_{\text{AVE}(X \rightarrow Y)}^{nm}(0)$.

The estimator (10) is constructed from a reduced dataset. The used data exclusion criterion is not independent of the assumed hidden confounders (i.e., the distribution of the hidden variables is expected to differ between the reduced data and the original data), and therefore results in a biased estimator. Under additional assumptions on the underlying LSCM, however, (10) may still be used to estimate T . We now give a population version argument. Assume that there is no interaction between X_s^t and H_s^t in the causal mechanism for Y_s^t , i.e., the function f in (2) splits into $f_1(X_s^t, \varepsilon_s^t) + f_2(H_s^t, \varepsilon_s^t)$. Then, the conditional expectation of $Y_s^t | (X_s^t, H_s^t)$ likewise splits additively into a function of X_s^t and a function of H_s^t . Using Proposition 5, it follows that any two different models for the marginal distribution of the latent process \mathbf{H} induce average causal effects $f_{\text{AVE}(X \rightarrow Y)}$ that are equal up to an additive constant. In particular, every model for \mathbf{H} induces the same value for T . By regarding the reduced dataset as a realization from a modified LSCM, in which the distribution of \mathbf{H} has been altered, this argument justifies the use of (10) as an estimator for T .⁴

4.3 Comparison with alternative assumptions on the causal structure

To emphasize the relevance of the assumed causal structure, we compare our method with two alternative approaches based on different assumptions about the ground truth: Model 1 assumes no confounders of (\mathbf{X}, \mathbf{Y}) and Model 2 assumes that the only confounder is the observed process \mathbf{W} (mean distance to a road). Even though none of the models may be a precise description of the data generating mechanism, we regard both Models 1 and 2 as less realistic than the LSCM. In both models we can, similarly to Definition 3, define the average causal effect of \mathbf{X} on \mathbf{Y} . Under Model 1, $f_{\text{AVE}(X \rightarrow Y)}$ coincides with the conditional expectation of Y_s^t given X_s^t , which can be estimated simply using sample averages (as is done in Figure 1 left). Under Model 2, $f_{\text{AVE}(X \rightarrow Y)}$ can, analogously to Proposition 5, be computed by adjusting for the confounder \mathbf{W} . For each $x \in \{0, 1\}$, we obtain an estimate $\hat{f}_{\text{AVE}(X \rightarrow Y)}^{nm}(x)$ by calculating sample averages of \mathbf{Y} across different subsets $\{(s, t) \in \mathbb{R}^2 \times \mathbb{N} : X_s^t = x, W_s^t \in \mathcal{W}_j\}, j \in \mathcal{J}$ (we here construct these by considering 100 equidistant quantiles of \mathbf{W}), and subsequently averaging over the resulting values. In both models, we further test the hypothesis of no causal effect of \mathbf{X} on \mathbf{Y} using approaches similar to the ones presented in Section 3. Under the LSCM assumption, we have constructed a permutation scheme that permutes the values of \mathbf{Y} along the time axis, to preserve the dependence between \mathbf{Y} and the assumed time-invariant confounders \mathbf{H} , see Proposition 11. Similarly, we construct a permutation scheme for Model 2 by permuting observations of \mathbf{Y} corresponding to similar values of the confounder \mathbf{W} (i.e., values within the same quantile range). Under the null hypothesis corresponding to Model 1, \mathbf{X} and \mathbf{Y} are (unconditionally) independent, and we therefore permute the values of \mathbf{Y} completely at random. Strictly speaking, the permutation schemes for Models 1 and 2 require additional exchangeability assumptions on \mathbf{Y} in order to yield valid resampling tests. In Appendix C, we repeat the analysis for Model 1 using a spatial block-permutation to account for the spatial dependence in \mathbf{Y} , and obtain similar results.

⁴In practice, we use the values of \mathbf{X} to exclude data points, and the above argument must thus be regarded a heuristic.

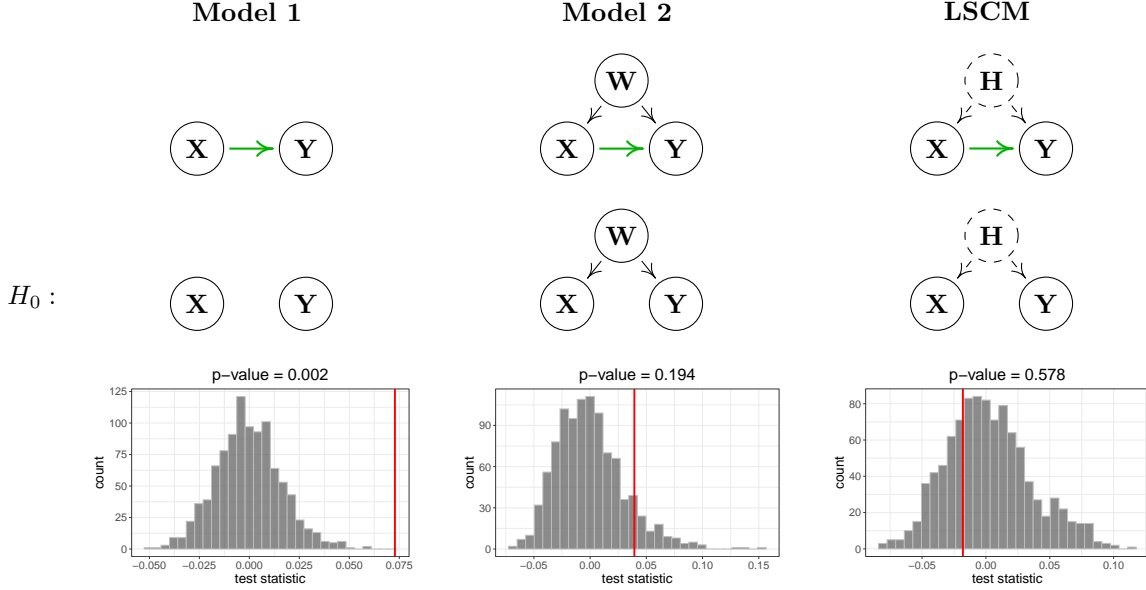


FIGURE 4. Testing for a causal influence of conflict (\mathbf{X}) on forest loss (\mathbf{Y}) using our method (right) and two alternative approaches (left and middle) which are based on different and arguably less realistic assumptions on the causal structure. The process \mathbf{W} corresponds to the mean distance to a road, and \mathbf{H} represents unobserved time-invariant confounders. Each of the above models gives rise to a different expression for the test statistic $\hat{T} = \hat{f}_{\text{AVE}(X \rightarrow Y)}^{nm}(1) - \hat{f}_{\text{AVE}(X \rightarrow Y)}^{nm}(0)$ (indicated by red vertical bars), see Sections 4.2 and 4.3. The gray histograms illustrate the empirical null distributions of \hat{T} under the respective null hypotheses obtained from 999 resampled datasets. The results show that our conclusions about the causal influence of conflict on forest loss strongly depend on the assumed causal structure: under Model 1, there is a positive, highly significant effect ($\hat{T} = 0.073$). When adjusting for the confounder \mathbf{W} , the effect size halves and becomes insignificant ($\hat{T} = 0.039$). When applying our proposed methodology, the estimated effect is negative ($\hat{T} = -0.018$).

4.4 Results

The results of applying our method and the two alternative approaches to the entire study region are depicted in Figure 4. Under Model 1, there is an enhancing, highly significant causal effect of conflict on forest loss ($\hat{T} = 0.073$, $P = 0.002$). When adjusting for transport infrastructure (quantified by \mathbf{W} , Model 2), the size of the estimated causal effect shrinks, and becomes insignificant ($\hat{T} = 0.039$, $P = 0.194$). (Note that we have considered other confounders, too, yet obtained similar results. For example, when adjusting for population density, which we consider as moderately temporally varying, we obtain $\hat{T} = 0.038$ and $P = 0.214$.) When applying the methodology proposed in this paper, that is, adjusting for all time-invariant confounders, the estimated effect swaps sign ($\hat{T} = -0.018$, $P = 0.578$), but is insignificant. One reason for this non-finding could be the time delay between the proposed cause (conflict) and effect (forest loss). To account for this potential issue, we also test for a causal effect of \mathbf{X} on \mathbf{Y} that is temporally lagged by one year, i.e., we use an estimator similar to (10), where we compare the average forest loss succeeding conflict events with the average forest loss succeeding non-conflict events. Again, the estimated influence of \mathbf{X} on \mathbf{Y} is negative and insignificant ($\hat{T} = -0.0293$, $P = 0.354$). Additionally, we perform alternative versions of the last two tests where we account for potential autocorrelation in the response variable, by adopting a temporal block-permutation scheme. In both cases, the test is insignificant, see Appendix C.

The above analysis provides an estimate for the average causal effect, see Equation (3), which, in

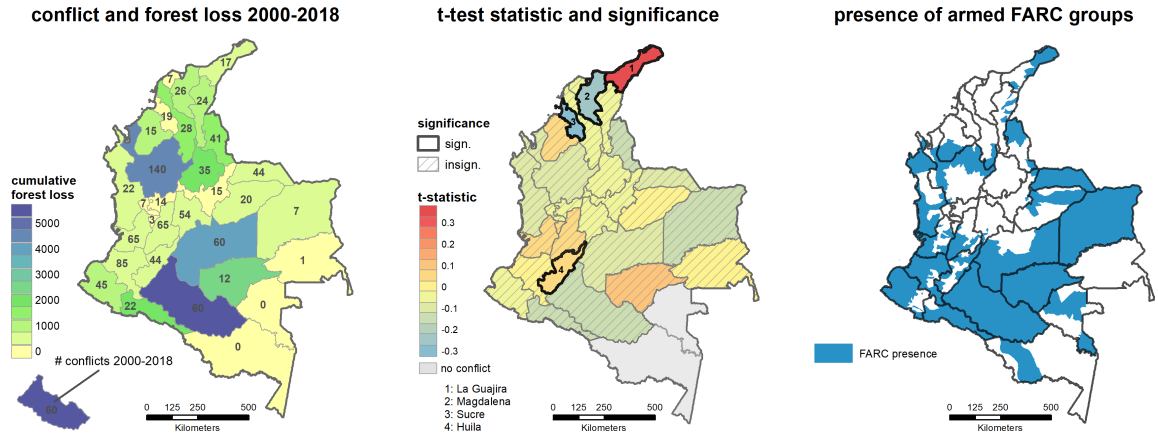


FIGURE 5. Regional analysis of conflict and forest loss in Colombia. The left panel shows the total forest loss and the total number of conflict events from 2000 to 2018 aggregated at department level. The most severe incidences of forest loss occur in the Northern Andean forests and on the northern borders of the Amazon region. In the middle panel, we report for each department estimates \hat{T} and test results for $H_0 : T = 0$, using the methodology described in Sections 2 and 3. We used a test level of $\alpha = 0.05$, and report significances without multiple-testing adjustment. In most departments, the estimated causal effect is negative (blue, conflict reduces forest loss), although mainly insignificant. We identify four departments with statistically significant results, hereof two with a positive causal effect (La Guajira and Huila) and two with a negative causal effect (Magdalena and Sucre). In total, there are 8 departments that are mostly controlled by FARC (above 75% FARC presence, right panel). Out of these, 6 departments have a negative test statistic (conflict reduces forest loss).

particular, averages over space. Given that Colombia is a country with high ambiental and socio-economic heterogeneity, where different regional dynamics may influence the causal relationship between conflict and forest loss, we further conduct an analysis at the department level (see Figure 5). In fact, there is considerable spatial variation in the estimated causal effects, with significant positive as well as negative effects (Figure 5 middle). From a modeling perspective, this variation may be seen as evidence for an interaction effect between conflict and the assumed hidden confounders. In most departments, the estimated causal effect is negative (although mostly insignificant), meaning that conflict tends to decrease forest loss. The strongest positive and significant causal influence is identified in the La Guajira department ($\hat{T} = 0.398$, $P = 0.047$). Although this region is commonly associated with semi-arid to very dry conditions, most conflicts occurred in the South-Western areas, at the beginning of Caribbean tropical forests (see Figure 1). In fact, these zones have also been also identified by Negret et al. [2019] as having been strongly affected by deforestation pressure in the wake of conflict. Interestingly, the neighboring Magdalena department shows the opposite effect ($\hat{T} = -0.218$, $P = 0.004$), which might point to a different socio-political reality. It may also reflect the fact that this department experienced high forest loss after the ceasefire in the entire Colombia [Prem et al., 2020]. The positive effect in the department of Huila ($\hat{T} = 0.095$, $P = 0.023$) is again in line with the findings by Negret et al. [2019] (based on a visual inspection of their attribution maps). Out of the 8 departments that are mostly controlled by FARC (Figure 5 right), 6 have a negative test statistic, meaning that conflict reduces forest loss. This can be explained in part by the internal governance of this group, where forest cover was a strategic advantage for both their own protection as well as for cocaine production. Overall, of course, the peace-induced acceleration of forest loss has to be discussed with caution, and should not be interpreted reversely as if conflict per se is a measure of environmental protection as it has been discussed, for instance, by Clerici et al. [2020].

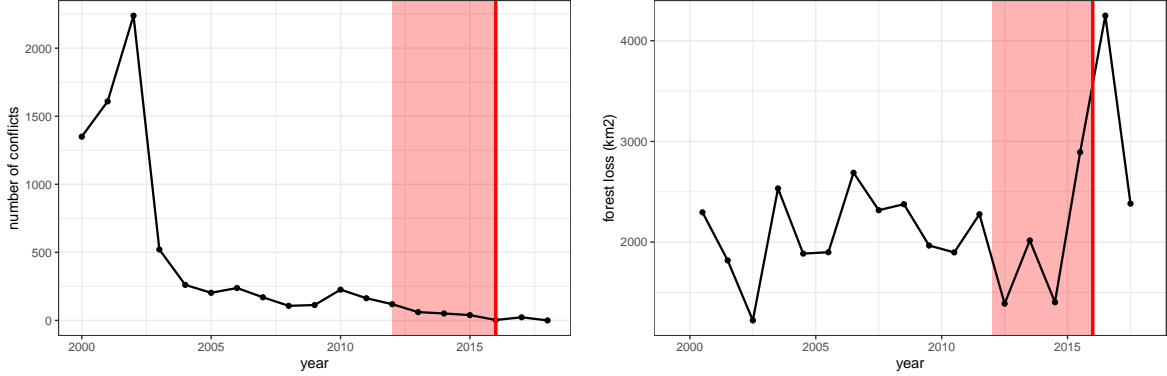


FIGURE 6. Total number of conflicts (left) and total forest loss (right) in the years 2000–2018 in Colombia. In the right panel, the height of the curve at $x + 0.5$ corresponds to the total forest loss between years x and $x + 1$. The shaded area marks the Colombian peace process, which began in September 2012. A final agreement was reached in October 2016 (vertical red line).

4.5 Interpretation of our results in light of the Colombian peace process

In late 2012, negotiations that later would be known as “Colombian peace process” started between the then president of Colombia and the strongest group of rebels, the FARC, and lasted until 2016. Controversies in the country culminated in the rejection of the agreement in a national referendum. Despite this failure, peace was declared by both parties upon a revised agreement in October 2016, and became effective in the subsequent year.⁵ While severe incidences continued to occur in the year leading up to the final agreement, the negotiations marked a steadily decreasing number of conflicts, see Figure 6 (left). Since this decrease of conflicts is the consequence of governmental intervention, rather than a natural resolution of local tensions, the peace process provides an opportunity to verify the intervention effects estimated in Section 4.4. As can be seen in Figure 6 (right), Colombia experienced a steep increase in the total forest loss in the final phase of the peace negotiations. Although there may be several other factors which have contributed to this development, we observe that these results align with our previous finding of an overall negative causal effect of conflict on forest loss ($\hat{T} < 0$).

5 Conclusions and future work

5.1 Methodology

This paper introduces ways to discuss causal inference for spatio-temporal data. From a methodological perspective, it contains three main contributions: the definition of a class of causal models for multivariate spatio-temporal stochastic processes, a procedure for estimating causal effects within this model class, and a non-parametric hypothesis test for the overall existence of such effects. Our method allows for the influence of arbitrarily many latent confounders, as long as these confounders do not vary across time (or space). We prove asymptotic consistency of our estimator, and verify this finding empirically using simulated data. Our results hold under weak assumptions on the data generating process, and do not rely on any particular distributional properties of the data. We prove sufficient conditions under which these rather general assumptions hold true. The proposed testing procedure is based on data resampling and provably obtains valid level in finite samples.

Our work can be extended into several directions. We proved that Assumption A1 holds for regularly sampled stationary Gaussian processes. Such settings allow for the application of well-known theorems

⁵The agreement was signed only by the FARC, while other guerilla groups remain active.

about stationary and ergodic sequences. We hypothesize that the assumption also holds in the more general case, where the marginalized process does not resemble a (collection of) stationary sequence(s), as long certain mixing conditions are satisfied. For example, we believe that if the original spatial process \mathbf{H}^1 is weakly stationary and mixing, Assumption A1 holds under any spatial sampling scheme $(s_n)_{n \in \mathbb{N}}$ with $\|s_n\| \rightarrow \infty$ as $n \rightarrow \infty$.

In our method for estimating causal effects, we allow the regression model for (X_s^t, Y_s^t) to change arbitrarily (within the specified function class) between neighboring locations. It may be worthwhile exploring how smoothness assumptions on the hidden variables can be incorporated in the modeling process to gain statistical efficiency of the proposed estimator. Likewise, such smoothness assumptions would allow for alternative permutation schemes (data can be permuted spatially wherever \mathbf{H} is assumed to be constant) which could lead to increased power of our hypothesis tests.

5.2 Case study

We have applied our methodology to the problem of quantifying the causal influence of conflict on forest loss in Colombia. Conflict events are predictive of exceedances in forest loss, but we find no evidence of a causal relation when analyzing this problem on country level: once all (time-invariant) confounders are adjusted for, there is a negative but insignificant correlation between conflict and forest loss. Our analysis on department level suggests that this non-finding could be due to locally varying effects of opposite directionality, which would approximately cancel out in our final estimate. In most departments, we find negative (mostly insignificant) effect of conflict on forest loss, although we also identify a few departments where conflict seems to increase forest loss. The overall negative influence of conflict on forest loss estimated by our method is in line with the observation that in the final phase of the peace process, which stopped many of the existing conflicts, the total forest loss in Colombia has increased. However, these results should be interpreted with caution. Overall, we find that, once all time-invariant confounders are adjusted for, conflicts have only weak explanatory power for predicting forest loss, and the potential causal effect is therefore likely to be small, compared to other drivers of forest loss. The chain of events which link the occurrence of an armed conflict with the clearing of local forests is rather complex, and we hope that future research will be able to shed further light on the underlying causal relationship.

Acknowledgments

This work contributes to the Global Land Programme, and was supported by a research grant (18968) from VILLUM FONDEN. M.D.M. thanks the European Space Agency for funding the Earth System Data Lab. We are grateful to Steffen Lauritzen for helpful comments on ergodicity, and Niels Richard Hansen and Niklas Pfister for insightful discussions on the sufficiency conditions in Section 2.3.2. We further thank Lina Estupinan-Suarez and Alejandro Salazar for helpful discussions on the environmental impacts of the Colombian peace process.

A Examples

Let $(\mathbf{X}, \mathbf{Y}, \mathbf{H})$ come from an LSCM satisfying condition (L1) described in Section 2.3.2. Below, we give two examples of distributions over (\mathbf{X}, \mathbf{H}) for which also conditions (L2) and (L3) hold true. In both cases, $\frac{1}{m}(\Phi_s^m)^\top \Phi_s^m$ converges in probability to some limit matrix of the form $\mathbb{E}_\nu[\varphi(X)\varphi(X)^\top]$ for some measure ν with full support on \mathbb{R}^d . To see that $\mathbb{E}_\nu[\varphi(X)\varphi(X)^\top]$ is strictly positive definite, let $v \in \mathbb{R}^p$ be such that $0 = v^\top \mathbb{E}_\nu[\varphi(X)\varphi(X)^\top]v = \mathbb{E}_\nu[\|\varphi(X)^\top v\|_2^2]$. By continuity of φ , it follows that $\varphi^\top v \equiv 0$, and the linear independence of $\varphi_1, \dots, \varphi_p$ implies that $v = 0$.

Example 13 (Temporally ergodic \mathbf{X}). Let $(\mathbf{X}, \mathbf{Y}, \mathbf{H})$ come from an LSCM satisfying Assumption (L1). Assume that for every $\mathbf{h} \in \mathcal{H}$ and $s \in \mathbb{R}^2$, it holds that under $\mathbb{P}_{\mathbf{h}}$, \mathbf{X}_s is a stationary and mixing process with a marginal distribution that has full support on \mathbb{R}^d (e.g., a vector autoregressive process with additive Gaussian noise). Assume further that $\mathbb{E}_{\mathbf{h}}[|\xi_s^1|^2] < \infty$ and $\mathbb{E}_{\mathbf{h}}[|\varphi_i(X_s^1)|^2] < \infty$ for all $i \in \{1, \dots, p\}$. Analogously to the proof of Proposition 8, we can then show that for each $i, j \in \{1, \dots, p\}$, the sequences $(\varphi_i(X_s^t)\xi_s^t)_{t \in \mathbb{N}}$ and $(\varphi_i(X_s^t)\varphi_j(X_s^t))_{t \in \mathbb{N}}$ are ergodic under $\mathbb{P}_{\mathbf{h}}$, and it follows that

$$\left(\frac{1}{m}(\Phi_s^m)^\top \xi_s^m\right)_i = \frac{1}{m} \sum_{t=1}^m \varphi_i(X_s^t)\xi_s^t \rightarrow \mathbb{E}_{\mathbf{h}}[\varphi_i(X_s^1)\xi_s^1]$$

and

$$\left(\frac{1}{m}(\Phi_s^m)^\top \Phi_s^m\right)_{ij} = \frac{1}{m} \sum_{t=1}^m \varphi_i(X_s^t)\varphi_j(X_s^t) \rightarrow \mathbb{E}_{\mathbf{h}}[\varphi_i(X_s^1)\varphi_j(X_s^1)]$$

as $m \rightarrow \infty$ in probability under $\mathbb{P}_{\mathbf{h}}$. Since for all $s \in \mathbb{R}^2$, $\mathbb{E}_{\mathbf{h}}[\varphi(X_s^1)\xi_s^1] = \mathbb{E}_{\mathbf{h}}[\varphi(X_s^1)] \cdot \mathbb{E}_{\mathbf{h}}[\xi_s^1] = 0$ and $\mathbb{E}_{\mathbf{h}}[\varphi(X_s^1)\varphi(X_s^1)^\top] \succ 0$, the above implies (L2) and (L3).

Example 14 (Temporally independent \mathbf{X} with convergent mixture distributions). Let $(\mathbf{X}, \mathbf{Y}, \mathbf{H})$ come from an LSCM satisfying Assumption (L1) for some bounded functions $\varphi_1, \dots, \varphi_p$. Assume that for every $s \in \mathbb{R}^2$, the variables X_s^1, X_s^2, \dots are conditionally independent given \mathbf{H} (they are not required to be identically distributed), and that for every $\mathbf{h} \in \mathcal{H}$, the sequence of mixture distributions

$$\mathbb{P}_{s, \mathbf{h}}^m := \frac{1}{m} \sum_{t=1}^m \mathbb{P}_{X_s^t | \mathbf{H}=\mathbf{h}}, \quad m \in \mathbb{N}, \quad (11)$$

converges, for $m \rightarrow \infty$, weakly towards some limit measure $\mathbb{P}_{s, \mathbf{h}}^\infty$ with full support on \mathbb{R}^d . Then, conditions (L1) and (L2) are satisfied. To see this, let $\mathbf{h} \in \mathcal{H}$ and $s \in \mathbb{R}^2$ be fixed for the rest of this example. Let $m \in \mathbb{N}$ and $\delta > 0$. Since $\mathbb{E}_{\mathbf{h}}[(\Phi_s^m)^\top \xi_s^m] = 0$, it follows from Chebychev's inequality that for all $i \in \{1, \dots, p\}$,

$$\mathbb{P}_{\mathbf{h}}(|\frac{1}{m}((\Phi_s^m)^\top \xi_s^m)_i| > \delta) \leq \frac{1}{\delta^2} \text{Var}_{\mathbf{h}}\left(\frac{1}{m}((\Phi_s^m)^\top \xi_s^m)_i\right) = \frac{\mathbb{E}_{\mathbf{h}}((\xi_s^1)^2)}{\delta^2 m} \underbrace{\mathbb{E}_{s, \mathbf{h}}^m[\varphi_i(X)^2]}_{\text{unif. bounded}} \rightarrow 0 \quad \text{as } m \rightarrow \infty,$$

showing that (L2) is satisfied. To prove (L3), let $M^m := \mathbb{E}_{s, \mathbf{h}}^m[\varphi(X)\varphi(X)^\top]$, $m \in \mathbb{N}$, and $M^\infty := \mathbb{E}_{s, \mathbf{h}}^\infty[\varphi(X)\varphi(X)^\top]$ (to simplify notation, we here omit the implicit dependence on \mathbf{h} and s). By assumption on $(\mathbb{P}_{s, \mathbf{h}}^m)_{m \in \mathbb{N}}$, M^m converges entrywise to M^∞ as $m \rightarrow \infty$. Together with another application of Chebychev's inequality, it follows that for all $i, j \in \{1, \dots, p\}$,

$$\begin{aligned} \mathbb{P}_{\mathbf{h}}(|\frac{1}{m}((\Phi_s^m)^\top \Phi_s^m)_{ij} - M_{ij}^\infty| > 2\delta) &\leq \mathbb{P}_{\mathbf{h}}(|\frac{1}{m}((\Phi_s^m)^\top \Phi_s^m)_{ij} - M_{ij}^m| > \delta) + \mathbb{P}_{\mathbf{h}}(|M_{ij}^m - M_{ij}^\infty| > \delta) \\ &\leq \frac{1}{\delta^2 m} \underbrace{\mathbb{E}_{s, \mathbf{h}}^m[\varphi_i(X)^2 \varphi_j(X)^2]}_{\text{unif. bounded}} + \underbrace{\mathbb{P}_{\mathbf{h}}(|M_{ij}^m - M_{ij}^\infty| > \delta)}_{=0 \text{ for } m \text{ large}} \\ &\rightarrow 0 \quad \text{as } m \rightarrow \infty, \end{aligned}$$

showing that $\frac{1}{m}((\Phi_s^m)^\top \Phi_s^m)$ converges entrywise to $M^\infty \succ 0$ in probability under $\mathbb{P}_{\mathbf{h}}$, and (L3) follows.

Remark 15 (Necessity of the convergence of mixtures). The convergence assumption on $\mathbb{P}_{s, \mathbf{h}}^m$ is crucial for obtaining the above consistency result. It is easy to construct examples of $(\mathbb{P}_{X_s^t | \mathbf{H}=\mathbf{h}})_{t \in \mathbb{N}}$ where this assumption fails to hold. For example, let $\mathbb{P}_{\mathbf{h}}(X_s^t \in (-\infty, -1]^d) = 1$ whenever $\lfloor \log_2 t \rfloor$ is even, and $\mathbb{P}_{\mathbf{h}}(X_s^t \in [1, \infty)^d) = 1$ whenever $\lfloor \log_2 t \rfloor$ is odd. This construction is visualized in Figure 7. Then, both sequences $(\mathbb{P}_{\mathbf{h}}(X_s^t \in (-\infty, -1]^d))_{t \in \mathbb{N}}$ and $(\mathbb{P}_{\mathbf{h}}(X_s^t \in [1, \infty)^d))_{t \in \mathbb{N}}$ alternate between zero and one, with a frequency chosen such that for all $k \geq 2$ even, $\mathbb{P}_{s, \mathbf{h}}^{2^k-1}([1, \infty)^d) = 2/3$, and for all $k \geq 3$ odd, $\mathbb{P}_{s, \mathbf{h}}^{2^k-2}((-\infty, -1]^d) = 2/3$, showing that $\mathbb{P}_{s, \mathbf{h}}^m$ does not converge. In this case, the dataset $\{(X_s^t, Y_s^t) :$

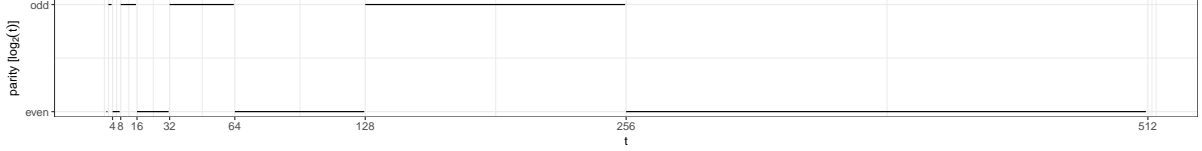


FIGURE 7. Visualization of the example in Remark 15. Whenever the parity of $\lfloor \log_2 t \rfloor$ changes from even to odd, the entire mass of $\mathbb{P}_{X_s^t | \mathbf{H}=\mathbf{h}}$ moves from $(-\infty, -1]^d$ to $[1, \infty)^d$, and vice versa. In this case, the mixture $\mathbb{P}_{s,\mathbf{h}}^m$ in (11) does not converge, and the consistency in Proposition 9 does not hold in general.

$t \in \{1, \dots, m\}$ alternates between mostly containing pairs (X_s^t, Y_s^t) with $X_s^t \in (-\infty, -1]^d$ and mostly containing pairs (X_s^t, Y_s^t) with $X_s^t \in [1, \infty)^d$. If the functional dependence of Y_s^t on X_s^t differs between these two domains, the estimator $\hat{f}_{Y|X}^m$ does therefore not converge in general.

Remark 16 (Conditions implying the convergence of mixtures). *We can make the convergence assumption on $\mathbb{P}_{s,\mathbf{h}}^m$ more concrete in the case where the distributions in $(\mathbb{P}_{X_s^t | \mathbf{H}=\mathbf{h}})_{t \in \mathbb{N}}$ differ only in their respective mean vectors. Assume there exist functions $\mu_s^t : \mathcal{Z}_\ell \rightarrow \mathbb{R}^d$ and $g_s : \mathcal{Z}_\ell \times \mathbb{R}^d \rightarrow \mathbb{R}^d$, $(s, t) \in \mathbb{R}^2 \times \mathbb{N}$, and a d -dimensional error process $\zeta \perp \mathbf{H}$, such that for each $s \in \mathbb{R}^2$, $\zeta_s^1, \zeta_s^2, \dots$ are i.i.d., and such that for all $(s, t) \in \mathbb{R}^2 \times \mathbb{N}$ it holds that $X_s^t = \mu_s^t(\mathbf{H}) + g_s(\mathbf{H}, \zeta_s^t)$. Assume further that for each $\mathbf{h} \in \mathcal{H}$ and $s \in \mathbb{R}^2$, $g_s(\mathbf{h}, \zeta_s^0)$ has strictly positive density $f_{s,\mathbf{h}}$ w.r.t. the Lebesgue measure on \mathbb{R}^d . We can then ensure convergence of the mixture distributions $\mathbb{P}_{s,\mathbf{h}}^m$ by requiring that for each $\mathbf{h} \in \mathcal{H}$ and $s \in \mathbb{R}^2$ there exists some density function $f_{s,\mathbf{h}}^{mix}$ on \mathbb{R}^d , such that for all $x \in \mathbb{R}^d$ it holds that⁶*

$$\lim_{m \rightarrow \infty} \frac{1}{m} \sum_{t=1}^m \mathbb{1}_{(-\infty, x]}(\mu_s^t(\mathbf{h})) = \int_{(-\infty, x]} f_{s,\mathbf{h}}^{mix}(z) dz.$$

(Intuitively, this equation states that, in the limit $m \rightarrow \infty$, the set $\{\mu_s^t(\mathbf{h}) : t \in \{1, \dots, m\}\}$ looks like an i.i.d. sample drawn from the distribution with density $f_{s,\mathbf{h}}^{mix}$.) For all $\mathbf{h} \in \mathcal{H}$, $s \in \mathbb{R}^2$, $m \in \mathbb{N}$ and $x \in \mathbb{R}^d$, we then have

$$\begin{aligned} \mathbb{P}_{s,\mathbf{h}}^m((-\infty, x]) &= \frac{1}{m} \sum_{t=1}^m \int_{(-\infty, x]} f_{s,\mathbf{h}}(v - \mu_s^t(\mathbf{h})) dv \\ &= \int_{\mathbb{R}^d} \frac{1}{m} \sum_{t=1}^m f_{s,\mathbf{h}}(v - \mu_s^t(\mathbf{h})) \mathbb{1}_{(-\infty, x]}(v) dv \\ &= \int_{\mathbb{R}^d} f_{s,\mathbf{h}}(v) \frac{1}{m} \sum_{t=1}^m \mathbb{1}_{(-\infty, x-v]}(\mu_s^t(\mathbf{h})) dv, \end{aligned}$$

and it follows from the dominated convergence theorem that

$$\begin{aligned} \lim_{m \rightarrow \infty} \mathbb{P}_{s,\mathbf{h}}^m((-\infty, x]) &= \int_{\mathbb{R}^k} f_{s,\mathbf{h}}(v) \int_{(-\infty, x-v]} f_{s,\mathbf{h}}^{mix}(z) dz dv \\ &= \int_{(-\infty, x]} \int_{\mathbb{R}^k} f_{s,\mathbf{h}}(v) f_{s,\mathbf{h}}^{mix}(z - v) dv dz \\ &= \int_{(-\infty, x]} (f_{s,\mathbf{h}} * f_{s,\mathbf{h}}^{mix})(z) dz, \end{aligned}$$

showing that $\mathbb{P}_{s,\mathbf{h}}^m$ converges weakly to the measure with the convoluted density $f_{s,\mathbf{h}} * f_{s,\mathbf{h}}^{mix}$. Since $f_{s,\mathbf{h}}$ is strictly positive, this measure has full support on \mathbb{R}^d .

⁶By slight abuse of notation, we use $(-\infty, x]$ to denote the product set $\times_{i=1}^d (-\infty, x_i]$.

B Proofs

B.1 Proof of Proposition 4

By definition, intervening on \mathbf{X} leaves the conditional distribution $\mathbf{Y} | (\mathbf{X}, \mathbf{H})$ unchanged. Under \mathbb{P}_x , the property (2) therefore still holds for the same error process ε . Since also the marginal distribution of \mathbf{H} is unaffected by the intervention, we have that

$$\mathbb{E}_{\mathbb{P}_x}[Y_s^t] = \mathbb{E}_{\mathbb{P}_x}[f(X_s^t, H_s^t, \varepsilon_s^t)] = \mathbb{E}_{\mathbb{P}_x}[f(x, H_s^t, \varepsilon_s^t)] = \mathbb{E}[f(x, H_s^t, \varepsilon_s^t)] = \mathbb{E}[f(x, H_0^1, \varepsilon_0^1)] = f_{\text{AVE}(X \rightarrow Y)}(x),$$

as desired. \square

B.2 Proof of Theorem 7

Consider a fixed $x \in \mathcal{X}$. For every $n, m \in \mathbb{N}$ we have that

$$\begin{aligned} \hat{f}_{\text{AVE}(X \rightarrow Y)}^{nm}(\mathbf{X}_n^m, \mathbf{Y}_n^m)(x) - f_{\text{AVE}(X \rightarrow Y)}(x) &= \frac{1}{n} \sum_{i=1}^n \hat{f}_{Y|X}^m(\mathbf{X}_{s_i}^m, \mathbf{Y}_{s_i}^m)(x) - \mathbb{E}[f_{Y|(X,H)}(x, H_0^1)] \\ &= \frac{1}{n} \sum_{i=1}^n \left(\hat{f}_{Y|X}^m(\mathbf{X}_{s_i}^m, \mathbf{Y}_{s_i}^m)(x) - f_{Y|(X,H)}(x, H_{s_i}^1) \right) \\ &\quad + \frac{1}{n} \sum_{i=1}^n f_{Y|(X,H)}(x, H_{s_i}^1) - \mathbb{E}[f_{Y|(X,H)}(x, H_0^1)] \\ &= r_1(\mathbf{X}_n^m, \mathbf{Y}_n^m, \mathbf{H}_n^1) + r_2(\mathbf{H}_n^1), \end{aligned}$$

where

$$\begin{aligned} r_1(\mathbf{X}_n^m, \mathbf{Y}_n^m, \mathbf{H}_n^1) &:= \frac{1}{n} \sum_{i=1}^n \left(\hat{f}_{Y|X}^m(\mathbf{X}_{s_i}^m, \mathbf{Y}_{s_i}^m)(x) - f_{Y|(X,H)}(x, H_{s_i}^1) \right) \text{ and} \\ r_2(\mathbf{H}_n^1) &:= \frac{1}{n} \sum_{i=1}^n f_{Y|(X,H)}(x, H_{s_i}^1) - \mathbb{E}[f_{Y|(X,H)}(x, H_0^1)]. \end{aligned}$$

It follows that for any $\delta > 0$,

$$\mathbb{P} \left(\left| \hat{f}_{\text{AVE}(X \rightarrow Y)}^{nm}(\mathbf{X}_n^m, \mathbf{Y}_n^m)(x) - f_{\text{AVE}(X \rightarrow Y)}^0(x) \right| > \delta \right) \leq \mathbb{P}(|r_1(\mathbf{X}_n^m, \mathbf{Y}_n^m, \mathbf{H}_n^1)| > \delta/2) + \mathbb{P}(|r_2(\mathbf{H}_n^1)| > \delta/2).$$

Let now $\alpha > 0$ be arbitrary. By Assumption A1, there exists $N \in \mathbb{N}$ such that for all $n \geq N$, $\mathbb{P}(|r_2(\mathbf{H}_n^1)| \geq \delta/2) \leq \alpha/2$. By Assumption A2, we can for any such $n \geq N$ find $M_n \in \mathbb{N}$, such that for all $i = 1, \dots, n$ and all $m \geq M_n$ it holds that $\mathbb{P}(|\hat{f}_{Y|X}^m(\mathbf{X}_{s_i}^m, \mathbf{Y}_{s_i}^m)(x) - f_{Y|(X,H)}(x, H_{s_i}^1)| > \delta/2) \leq \alpha/(2n)$. For all $m \geq M_n$ we then have

$$\begin{aligned} \mathbb{P}(|r_1(\mathbf{X}_n^m, \mathbf{Y}_n^m, \mathbf{H}_n^1)| > \delta/2) &\leq \mathbb{P} \left(\frac{1}{n} \sum_{i=1}^n \left| \hat{f}_{Y|X}^m(\mathbf{X}_{s_i}^m, \mathbf{Y}_{s_i}^m)(x) - f_{Y|(X,H)}(x, H_{s_i}^1) \right| > \delta/2 \right) \\ &\leq \mathbb{P} \left(\bigcup_{i=1}^n \left\{ \left| \hat{f}_{Y|X}^m(\mathbf{X}_{s_i}^m, \mathbf{Y}_{s_i}^m)(x) - f_{Y|(X,H)}(x, H_{s_i}^1) \right| > \delta/2 \right\} \right) \\ &\leq \sum_{i=1}^n \mathbb{P} \left(\left| \hat{f}_{Y|X}^m(\mathbf{X}_{s_i}^m, \mathbf{Y}_{s_i}^m)(x) - f_{Y|(X,H)}(x, H_{s_i}^1) \right| > \delta/2 \right) \\ &\leq \sum_{i=1}^n \alpha/(2n) = \alpha/2, \end{aligned}$$

and the result follows. \square

B.3 Proof of Proposition 8

By construction, $(H_{s_n}^1)_{n \in \mathbb{N}}$ can be decomposed into m subsequences $(H_{s_{(n-1)m+j}}^1)_{n \in \mathbb{N}}$, $j \in \{1, \dots, m\}$, each of which corresponds to an equally spaced sampling of \mathbf{H}^1 along the first spatial axis. We first prove that each of these subsequences satisfies Assumption A1, and then conclude that the same must hold for the original sequence $(H_{s_n}^1)_{n \in \mathbb{N}}$. Let $j \in \{1, \dots, m\}$ and let $\varphi : \mathbb{R}^\ell \rightarrow \mathbb{R}$ be a measurable function with $\mathbb{E}[|\varphi(H_0^1)|] < \infty$. For notational simplicity, let for each $n \in \mathbb{N}$, $Z_n := H_{s_{(n-1)m+j}}^1$. The idea is to apply an ergodic theorem for real-valued stationary and ergodic time series [e.g., Rønn-Nielsen and Sokol, 2013, Corollary 2.3.13] to the sequence $(\varphi(Z_n))_{n \in \mathbb{N}}$. By stationarity of the process \mathbf{H}^1 , and by choice of the sampling scheme, $(\varphi(Z_n))_{n \in \mathbb{N}}$ is indeed stationary. We need to show that $(\varphi(Z_n))_{n \in \mathbb{N}}$ is also ergodic. Using Rønn-Nielsen and Sokol [2013, Lemma 2.3.15], this follows by proving the following mixing condition: for all $p, q \geq 1$ and all $A_1, \dots, A_p \in \mathcal{B}(\mathbb{R})$ and $B_1, \dots, B_q \in \mathcal{B}(\mathbb{R})$, it holds that

$$\begin{aligned} & \mathbb{P}(\varphi(Z_1) \in A_1, \dots, \varphi(Z_p) \in A_p, \varphi(Z_{n+1}) \in B_1, \dots, \varphi(Z_{n+p}) \in B_q) \\ & \rightarrow \mathbb{P}(\varphi(Z_1) \in A_1, \dots, \varphi(Z_p) \in A_p) \cdot \mathbb{P}(\varphi(Z_1) \in B_1, \dots, \varphi(Z_q) \in B_q) \quad \text{as } n \rightarrow \infty. \end{aligned} \quad (12)$$

Since the finite-dimensional distributions of $(Z_n)_{n \in \mathbb{N}}$ are Gaussian, this condition is easily verified. Let $p, q \geq 1$, and let $\mathbb{P}_1 = \mathcal{N}(\mu_1, \Sigma_1)$ and $\mathbb{P}_2 = \mathcal{N}(\mu_2, \Sigma_2)$ be the distributions of (Z_1, \dots, Z_p) and (Z_1, \dots, Z_q) , respectively. Property (12) follows if we can show that $(Z_1, \dots, Z_m, Z_{n+1}, \dots, Z_{n+p})$ converges to $\mathbb{P}_1 \otimes \mathbb{P}_2 = \mathcal{N}((\mu_1, \mu_2), \text{diag}(\Sigma_1, \Sigma_2))$ in distribution as $n \rightarrow \infty$. Convergence of the mean vector is trivial, and convergence of the covariance matrix follows by the assumption on C and our choice of spatial sampling (the distance between the respective locations at which (Z_1, \dots, Z_m) and $(Z_{n+1}, \dots, Z_{n+p})$ are observed tends to infinity as n increases). To prove that the limit distribution is indeed Gaussian, one can then consider characteristic functions and apply a combination of Levy's Continuity Theorem [e.g., Williams, 1991, Theorem 18.1] and the Cramér-Wold Theorem [Cramér and Wold, 1936]. This proves that $\frac{1}{n} \sum_{i=1}^n \varphi(Z_i) \rightarrow \mathbb{E}[\varphi(Z_1)]$ in probability as $n \rightarrow \infty$, i.e., the subsequence $(H_{s_{(n-1)m+j}}^1)_{n \in \mathbb{N}}$ satisfies Assumption A1. Since j was arbitrary, this holds true for all $j \in \{1, \dots, m\}$. It remains to prove that also the original sequence $(H_{s_n}^1)_{n \in \mathbb{N}}$ satisfies Assumption A1.

Let an integrable function $\varphi : \mathbb{R}^\ell \rightarrow \mathbb{R}$ be given, and assume first that $\mathbb{E}[\varphi(H_0^1)] = 0$. For every $j \in \{1, \dots, m\}$ and $i \in \mathbb{N}$, define $S_i^j := \sum_{k=1}^i \varphi(H_{s_{(k-1)m+j}}^1)$. By the first part of the proof, we have that for all j , $\frac{1}{i} S_i^j \rightarrow 0$ in probability as $i \rightarrow \infty$. We want to show that also $\frac{1}{n} \sum_{k=1}^n \varphi(H_{s_k}^1) \rightarrow 0$ in probability as $n \rightarrow \infty$. Let $\delta, \alpha > 0$ and choose $I \in \mathbb{N}$ such that for all $j \in \{1, \dots, m\}$ and $i \geq I$, $\mathbb{P}(\frac{1}{i} |S_i^j| > \delta/m) \leq \alpha/m$. Define $N := mI + 1$ and pick an arbitrary $n \geq N$. We can then write $n = im + j$ for some $i \geq I$ and $j \in \{1, \dots, m\}$. With $J_1 := \{1, \dots, j\}$ and $J_2 = \{1, \dots, m\} \setminus J_1$, we then have

$$\begin{aligned} \mathbb{P}\left(\frac{1}{n} \left| \sum_{k=1}^n \varphi(H_{s_k}^1) \right| > \delta\right) &= \mathbb{P}\left(\frac{1}{n} \left| \sum_{j' \in J_1} S_{i+1}^{j'} + \sum_{j' \in J_2} S_i^{j'} \right| > \delta\right) \leq \mathbb{P}\left(\sum_{j' \in J_1} \frac{1}{i+1} |S_{i+1}^{j'}| + \sum_{j' \in J_2} \frac{1}{i} |S_i^{j'}| > \delta\right) \\ &\leq \sum_{j' \in J_1} \mathbb{P}\left(\frac{1}{i+1} |S_{i+1}^{j'}| > \delta/m\right) + \sum_{j' \in J_2} \mathbb{P}\left(\frac{1}{i} |S_i^{j'}| > \delta/m\right) \leq \alpha, \end{aligned}$$

which completes the proof in the case where $\mathbb{E}[\varphi(H_0^1)] = 0$. The general case follows by applying the above result to the function $\tilde{\varphi} = \varphi - \mathbb{E}[\varphi(H_0^1)]$. \square

B.4 Proof of Proposition 9

Let $s \in \mathbb{R}^2$ and $\mathbf{h} \in \mathcal{H}$. With $\gamma_s := f_1(h_s^1)$, it follows from (L1) that for all x and t , we have $\mathbb{E}[Y_s^t | X_s^t = x, H_s^t = h_s^t] = \varphi(x)^\top \gamma_s$. It therefore suffices to prove that $\hat{\gamma}_s^m \rightarrow \gamma_s$ in probability under $\mathbb{P}_{\mathbf{h}}$. For the ease of notation, we omit all sub- and superscripts from \mathbf{Y}_s^m , Φ_s^m and ξ_s^m in the below calculations. Let

$c > 0$ be such that (L3) holds true and let $\delta > 0$ be arbitrary. For every $m \in \mathbb{N}$, we then have

$$\begin{aligned}
\mathbb{P}_{\mathbf{h}}(\|\gamma_s - \hat{\gamma}_s^m\|_2 > \delta) &= \mathbb{P}_{\mathbf{h}}(\|\gamma_s - (\Phi^\top \Phi)^{-1} \Phi^\top \mathbf{Y}\|_2 > \delta) \\
&= \mathbb{P}_{\mathbf{h}}(\|\gamma_s - (\Phi^\top \Phi)^{-1} \Phi^\top (\Phi \gamma_s + \boldsymbol{\xi})\|_2 > \delta) \\
&= \mathbb{P}_{\mathbf{h}}(\|(\Phi^\top \Phi)^{-1} \Phi^\top \boldsymbol{\xi}\|_2 > \delta) \\
&\leq \mathbb{P}_{\mathbf{h}}(\|(\frac{1}{m} \Phi^\top \Phi)^{-1}\|_2 \|\frac{1}{m} \Phi^\top \boldsymbol{\xi}\|_2 > \delta) \\
&= \mathbb{P}_{\mathbf{h}}((\lambda_{\min}(\frac{1}{m} \Phi^\top \Phi))^{-1} \|\frac{1}{m} \Phi^\top \boldsymbol{\xi}\|_2 > \delta) \\
&= \mathbb{P}_{\mathbf{h}}((\lambda_{\min}(\frac{1}{m} \Phi^\top \Phi))^{-1} \|\frac{1}{m} \Phi^\top \boldsymbol{\xi}\|_2 > \delta \text{ and } \lambda_{\min}(\frac{1}{m} \Phi^\top \Phi) > c) \\
&\quad + \mathbb{P}_{\mathbf{h}}((\lambda_{\min}(\frac{1}{m} \Phi^\top \Phi))^{-1} \|\frac{1}{m} \Phi^\top \boldsymbol{\xi}\|_2 > \delta \text{ and } \lambda_{\min}(\frac{1}{m} \Phi^\top \Phi) \leq c) \\
&\leq \mathbb{P}_{\mathbf{h}}(\|\frac{1}{m} \Phi^\top \boldsymbol{\xi}\|_2 > c\delta) + \mathbb{P}_{\mathbf{h}}(\lambda_{\min}(\frac{1}{m} \Phi^\top \Phi) \leq c),
\end{aligned}$$

which tends to zero as $m \rightarrow \infty$ by (L2) and (L3). \square

B.5 Proof of Proposition 11

Recall our definition of $\mathcal{H} \subseteq \mathcal{Z}_\ell$ as the set of functions $\mathbf{h} : \mathbb{R}^2 \times \mathbb{N} \rightarrow \mathbb{R}^\ell$ that are constant in the time-argument. Since \mathbf{H} is time-invariant, we have that $\mathbb{P}(\mathbf{H} \in \mathcal{H}) = 1$. It therefore suffices to prove that for all $\mathbf{h} \in \mathcal{H}$, $(\mathbf{X}_n^m, \sigma(\mathbf{Y}_n^m)) \stackrel{d}{=} (\mathbf{X}_n^m, \mathbf{Y}_n^m)$ under $\mathbb{P}(\cdot | \mathbf{H} = \mathbf{h})$. Assume that H_0 holds true, and let σ be a permutation of $\{1, \dots, m\}$. Then, there exists a function $\tilde{f} : \mathbb{R}^{\ell+1} \rightarrow \mathbb{R}$ and an error process $\boldsymbol{\varepsilon} \perp (\mathbf{X}, \mathbf{H})$ such that for all $(s, t) \in \mathbb{R}^2 \times \mathbb{N}$, $Y_s^t = \tilde{f}(H_s, \boldsymbol{\varepsilon}_s^t)$. It follows that the conditional distribution of $\mathbf{Y} | (\mathbf{X}, \mathbf{H})$ does not depend on \mathbf{X} , and hence that \mathbf{X} and \mathbf{Y} are conditionally independent given \mathbf{H} . Further, since $\boldsymbol{\varepsilon}^1, \boldsymbol{\varepsilon}^2, \dots$ are i.i.d., we have that for all $\mathbf{h} \in \mathcal{H}$, $\mathbf{Y}^1, \dots, \mathbf{Y}^m$ are i.i.d. under $\mathbb{P}(\cdot | \mathbf{H} = \mathbf{h})$. For all $\mathbf{h} \in \mathcal{H}$, it therefore holds that $(\mathbf{X}_n^m, \sigma(\mathbf{Y}_n^m)) \stackrel{d}{=} (\mathbf{X}_n^m, \mathbf{Y}_n^m)$ under $\mathbb{P}(\cdot | \mathbf{H} = \mathbf{h})$, and the result follows. \square

C Further results on resampling tests

C.1 Temporal autocorrelation in the response variable

A central assumption of the LSCM model class is that the error process of \mathbf{Y} is independent over time. This assumption says that all dependencies between different temporal instances of \mathbf{Y} are induced via the covariates \mathbf{X} or the time-invariant confounders \mathbf{H} . In practice, there may be other time-varying conditions influencing forest loss, thereby inducing a temporal dependence in \mathbf{Y} which cannot be explained by (\mathbf{X}, \mathbf{H}) . In this case, the exchangeability property in Proposition 11, and therefore the level of our resampling test, is violated. To incorporate temporal autocorrelation in the response variable, we adopt a block-permutation scheme: we divide the period 2000–2018 into 6 blocks (2000–2002, 2003–2005, ..., 2016–2018), and perform a block-wise permutation of the data from \mathbf{Y} . This procedure leaves the within-block dependence structure in \mathbf{Y} intact. The results align with our previous findings: $P = 0.892$ for the test of an instantaneous effect, and $P = 0.498$ for the test of a temporally lagged effect (when using the same test statistics as in Section 4.4).

C.2 Spatial block-permutation scheme for Model 1

In Section 4.3, we describe alternative permutation schemes to test the null hypotheses in Models 1 and 2. Strictly speaking, we require additional exchangeability assumptions on \mathbf{Y} to ensure the validity of the corresponding resampling tests. Here, we investigate an alternative permutation scheme for Model 1. To account for the spatial autocorrelation in \mathbf{Y} , we adopt a spatial block-permutation: for every year 2000–2018, observations are grouped into blocks of size $100\text{km} \times 100\text{km}$. To obtain resampled datasets,

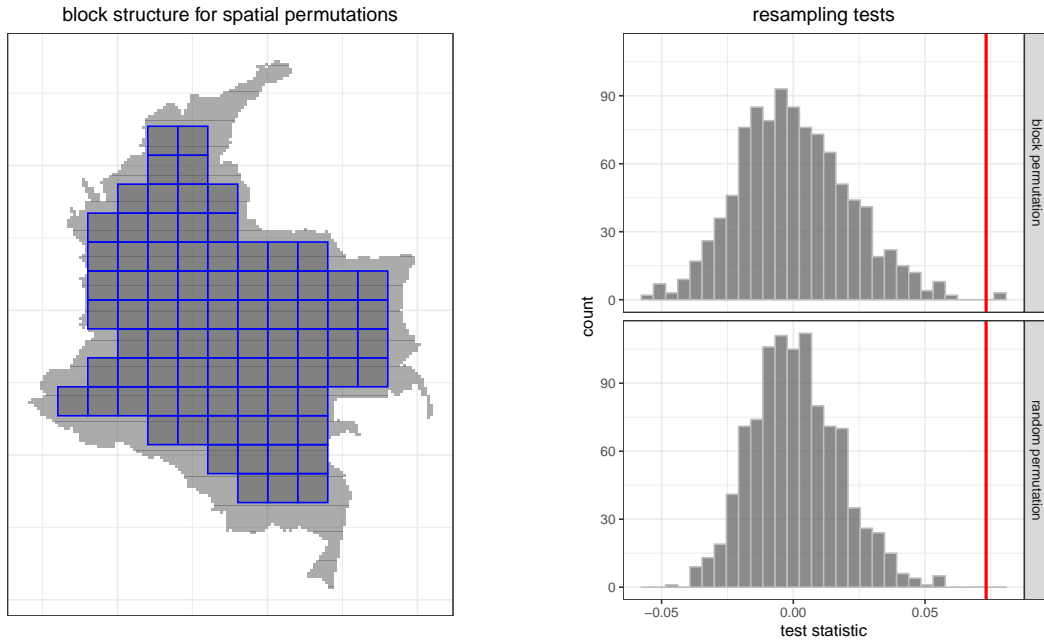


FIGURE 8. Block structure for the spatial permutation scheme (left) and results of resampling tests (right) for the null hypothesis in Model 1 from Section 4.4. The test statistic $\hat{T} = \hat{f}_{\text{AVE}(X \rightarrow Y)}^{nm}(1) - \hat{f}_{\text{AVE}(X \rightarrow Y)}^{nm}(0)$ is indicated by a red vertical bar. The empirical distribution of the test statistic under this permutation scheme (top right) has a higher variance than under the permutation scheme used in Section 4.4 (bottom right), resulting in a slightly larger p -value of 0.008 compared with the p -value of 0.002 for the original test. The significance of the test does not change.

we then permute values of \mathbf{Y} in these blocks of data, thereby leaving the spatial dependence within each block intact. Observations which do not fall in any of the blocks are permuted randomly. As seen in Figure 8, this procedure slightly increases the p -value, but does not affect the significance of the test.

References

- J. Aldrich. *Autonomy*. *Oxford Economic Papers*, 41:15–34, 1989.
- A. Angelsen and D. Kaimowitz. Rethinking the causes of deforestation: lessons from economic models. *The world bank research observer*, 14(1):73–98, 1999.
- M. Appel and E. Pebesma. On-demand processing of data cubes from satellite image collections with the gdalcubes library. *Data*, 4(3):92, 2019.
- D. Armenteras, E. Cabrera, N. Rodríguez, and J. Retana. National and regional determinants of tropical deforestation in Colombia. *Regional Environmental Change*, 13(6):1181–1193, 2013.
- D. Armenteras, L. Schneider, and L. M. Dávalos. Fires in protected areas reveal unforeseen costs of Colombian peace. *Nature ecology & evolution*, 3(1):20–23, 2019.
- V. Avitabile, M. Herold, G. B. Heuvelink, S. L. Lewis, O. L. Phillips, G. P. Asner, J. Armston, P. S. Ashton, L. Banin, N. Bayol, et al. An integrated pan-tropical biomass map using multiple reference datasets. *Global change biology*, 22(4):1406–1420, 2016.

- M. Baumann and T. Kuemmerle. The impacts of warfare and armed conflict on land systems. *Journal of land use science*, 11(6):672–688, 2016.
- M. Bertolacci, E. Cripps, O. Rosen, J. W. Lau, S. Cripps, et al. Climate inference on daily rainfall across the Australian continent, 1876–2015. *The Annals of Applied Statistics*, 13(2):683–712, 2019.
- K. A. Bollen. *Structural equations with latent variables*, volume 210. John Wiley & Sons, 2014.
- V. Butsic, M. Baumann, A. Shortland, S. Walker, and T. Kuemmerle. Conservation and conflict in the Democratic Republic of Congo: The impacts of warfare, mining, and protected areas on deforestation. *Biological conservation*, 191:266–273, 2015.
- K. M. Carlson, L. M. Curran, G. P. Asner, A. M. Pittman, S. N. Trigg, and J. M. Adeney. Carbon emissions from forest conversion by Kalimantan oil palm plantations. *Nature Climate Change*, 3(3):283–287, 2013.
- A. Castro-Nunez, O. Mertz, A. Buritica, C. C. Sosa, and S. T. Lee. Land related grievances shape tropical forest-cover in areas affected by armed-conflict. *Applied Geography*, 85:39–50, 2017.
- M. A. Chaplain, G. Singh, and J. C. McLachlan. *On growth and form: spatio-temporal pattern formation in biology*. Wiley, 1999.
- N. Clerici, D. Armenteras, P. Kareiva, R. Botero, J. Ramírez-Delgado, G. Forero-Medina, J. Ochoa, C. Pedraza, L. Schneider, C. Lora, et al. Deforestation in Colombian protected areas increased during post-conflict periods. *Scientific Reports*, 10(1):1–10, 2020.
- P. Collier et al. Economic causes of civil conflict and their implications for policy. Technical Report 76632, The World Bank, Washington, D.C., United States, 2000.
- H. Cramér and H. Wold. Some theorems on distribution functions. *Journal of the London Mathematical Society*, 1(4):290–294, 1936.
- N. Cressie and C. K. Wikle. *Statistics for spatio-temporal data*. John Wiley & Sons, 2015.
- M. Croicu and R. Sundberg. UCDP georeferenced event dataset codebook version 4.0. *Journal of Peace Research*, 50(4):523–532, 2015.
- L. M. Dávalos, K. M. Sanchez, and D. Armenteras. Deforestation and coca cultivation rooted in twentieth-century development projects. *BioScience*, 66(11):974–982, 2016.
- R. S. DeFries, T. Rudel, M. Uriarte, and M. Hansen. Deforestation driven by urban population growth and agricultural trade in the twenty-first century. *Nature Geoscience*, 3(3):178–181, 2010.
- K. M. Gaynor, K. J. Fiorella, G. H. Gregory, D. J. Kurz, K. L. Seto, L. S. Withey, and J. S. Brashares. War and wildlife: linking armed conflict to conservation. *Frontiers in Ecology and the Environment*, 14(10):533–542, 2016.
- A. E. Gelfand, H.-J. Kim, C. Sirmans, and S. Banerjee. Spatial modeling with spatially varying coefficient processes. *Journal of the American Statistical Association*, 98(462):387–396, 2003.
- E. Giorgi, P. J. Diggle, R. W. Snow, and A. M. Noor. Geostatistical methods for disease mapping and visualisation using data from spatio-temporally referenced prevalence surveys. *International Statistical Review*, 86(3):571–597, 2018.
- G. Giuliani, G. Camara, B. Killough, and S. Minchin. Earth observation open science: Enhancing reproducible science using data cubes, 2019.

- N. P. Gleditsch, H. Strand, M. Eriksson, M. Sollenberg, and P. Wallensteen. Armed conflict 1946–2001: A new dataset. *Journal of Peace Research*, 39:615–637, 2002.
- V. Gorsevski, E. Kasischke, J. Dempewolf, T. Loboda, and F. Grossmann. Analysis of the impacts of armed conflict on the Eastern Afromontane forest region on the South Sudan-Uganda border using multitemporal Landsat imagery. *Remote Sensing of Environment*, 118:10–20, 2012.
- C. W. Granger. Testing for causality: a personal viewpoint. *Journal of Economic Dynamics and control*, 2:329–352, 1980.
- T. Haavelmo. The probability approach in econometrics. *Econometrica*, 12:S1–S115 (supplement), 1944.
- A. R. Hall. *Generalized Method of Moments*. Advanced texts in econometrics. Oxford University Press, 2005.
- L. P. Hansen. Large sample properties of generalized method of moments estimators. *Econometrica*, 50(4):1029–1054, 1982.
- M. C. Hansen, P. V. Potapov, R. Moore, M. Hancher, S. A. Turubanova, A. Tyukavina, D. Thau, S. Stehman, S. J. Goetz, T. R. Loveland, et al. High-resolution global maps of 21st-century forest cover change. *Science*, 342(6160):850–853, 2013.
- A. Harrison. Blood timber: how Europe helped fund war in the Central African Republic: a report. <https://apo.org.au/node/55984>, 2015. Accessed: 2020-05-15.
- C. Hof, M. B. Araújo, W. Jetz, and C. Rahbek. Additive threats from pathogens, climate and land-use change for global amphibian diversity. *Nature*, 480(7378):516–519, 2011.
- S. Holly, M. H. Pesaran, and T. Yamagata. A spatio-temporal model of house prices in the USA. *Journal of Econometrics*, 158(1):160–173, 2010.
- L. C. Irland. State failure, corruption, and warfare: challenges for forest policy. *Journal of Sustainable Forestry*, 27(3):189–223, 2008.
- H. Kreft and W. Jetz. Global patterns and determinants of vascular plant diversity. *Proceedings of the National Academy of Sciences*, 104(14):5925–5930, 2007.
- E. F. Lambin and P. Meyfroidt. Global land use change, economic globalization, and the looming land scarcity. *Proceedings of the National Academy of Sciences*, 108(9):3465–3472, 2011.
- D. M. Landholm, P. Pradhan, and J. P. Kropp. Diverging forest land use dynamics induced by armed conflict across the tropics. *Global Environmental Change*, 56:86–94, 2019.
- S. L. Lauritzen. *Graphical models*, volume 17. Clarendon Press, 1996.
- P. Le Billon. The political ecology of transition in Cambodia 1989–1999: war, peace and forest exploitation. *Development and change*, 31(4):785–805, 2000.
- B. Liu, B. Huang, and W. Zhang. *Spatio-temporal analysis and optimization of land use/cover change: Shenzhen as a case study*. CRC Press, 2017.
- A. C. Lozano, H. Li, A. Niculescu-Mizil, Y. Liu, C. Perlich, J. Hosking, and N. Abe. Spatial-temporal causal modeling for climate change attribution. In *Proceedings of the 15th ACM SIGKDD international conference on Knowledge discovery and data mining*, pages 587–596, 2009.
- Q. Luo, W. Lu, W. Cheng, P. A. Valdes-Sosa, X. Wen, M. Ding, and J. Feng. Spatio-temporal Granger causality: A new framework. *NeuroImage*, 79:241–263, 2013.

- M. D. Mahecha, F. Gans, G. Brandt, R. Christiansen, S. E. Cornell, N. Fomferra, G. Kraemer, J. Peters, P. Bodesheim, G. Camps-Valls, et al. Earth system data cubes unravel global multivariate dynamics. *Earth System Dynamics Discussions*, 11:201–234, 2020.
- J.-M. Montero, G. Fernández-Avilés, and J. Mateu. *Spatial and spatio-temporal geostatistical modeling and kriging*, volume 998. John Wiley & Sons, 2015.
- S. Nativi, P. Mazzetti, and M. Craglia. A view-based model of data-cube to support big earth data systems interoperability. *Big Earth Data*, 1(1-2):75–99, 2017.
- P. J. Negret, J. Allan, A. Braczkowski, M. Maron, and J. E. Watson. Need for conservation planning in postconflict Colombia. *Conservation Biology*, 31, 2017.
- P. J. Negret, L. Sonter, J. E. Watson, H. P. Possingham, K. R. Jones, C. Suarez, J. M. Ochoa-Quintero, and M. Maron. Emerging evidence that armed conflict and coca cultivation influence deforestation patterns. *Biological Conservation*, 239:108176, 2019.
- W. K. Newey and D. McFadden. Large sample estimation and hypothesis testing. In *Handbook of Econometrics*, volume 4, pages 2111 – 2245. Elsevier, 1994.
- J. M. Pavía, B. Larraz, and J. M. Montero. Election forecasts using spatiotemporal models. *Journal of the American Statistical Association*, 103(483):1050–1059, 2008.
- J. Pearl. *Causality: models, reasoning and inference*, volume 29. Springer, 2 edition, 2009.
- T. R. Pearson, S. Brown, and F. M. Casarim. Carbon emissions from tropical forest degradation caused by logging. *Environmental Research Letters*, 9(3):034017, 2014.
- J. Peters, D. Janzing, and B. Schölkopf. *Elements of causal inference: foundations and learning algorithms*. MIT press, 2017.
- T. Pettersson and P. Wallensteen. Armed conflicts, 1946–2014. *Journal of peace research*, 52(4):536–550, 2015.
- N. Pfister, P. Bühlmann, B. Schölkopf, and J. Peters. Kernel-based tests for joint independence. *Journal of the Royal Statistical Society: Series B (Statistical Methodology)*, 80(1):5–31, 2018.
- M. Prem, S. Saavedra, and J. F. Vargas. End-of-conflict deforestation: Evidence from Colombias peace agreement. *World Development*, 129:104852, 2020.
- A. Rønn-Nielsen and A. Sokol. Advanced probability. <http://web.math.ku.dk/noter/filer/vidsand12.pdf>, 2013. Accessed: 2020-05-15.
- D. B. Rubin. Estimating causal effects of treatments in randomized and nonrandomized studies. *Journal of educational Psychology*, 66(5):688, 1974.
- A. M. Sánchez-Cuervo and T. M. Aide. Consequences of the armed conflict, forced human displacement, and land abandonment on forest cover change in Colombia: A multi-scaled analysis. *Ecosystems*, 16(6):1052–1070, 2013.
- A. M. Sánchez-Cuervo, T. M. Aide, M. L. Clark, and A. Etter. Land cover change in Colombia: surprising forest recovery trends between 2001 and 2010. *PloS one*, 7(8), 2012.
- M. Sherman. *Spatial statistics and spatio-temporal data: covariance functions and directional properties*. John Wiley & Sons, 2011.

- I. Shpitser, T. VanderWeele, and J. M. Robins. On the validity of covariate adjustment for estimating causal effects. In *Proceedings of the 26th Conference on Uncertainty in Artificial Intelligence, UAI 2010*, pages 527–536, Dec 2010. ISBN 9780974903965.
- L. J. Sonter, D. Herrera, D. J. Barrett, G. L. Galford, C. J. Moran, and B. S. Soares-Filho. Mining drives extensive deforestation in the Brazilian Amazon. *Nature Communications*, 8(1):1–7, 2017.
- E. J. Ward, J. E. Jannot, Y.-W. Lee, K. Ono, A. O. Shelton, and J. T. Thorson. Using spatiotemporal species distribution models to identify temporally evolving hotspots of species co-occurrence. *Ecological Applications*, 25(8):2198–2209, 2015.
- N. Wiener. The theory of prediction. In E. Beckenbach, editor, *Modern Mathematics for Engineers*. McGraw-Hill, New York, NY, 1956.
- C. K. Wikle, A. Zammit-Mangion, and N. Cressie. *Spatio-temporal Statistics with R*. CRC Press, 2019.
- D. Williams. *Probability with martingales*. Cambridge university press, 1991.
- A. Zammit-Mangion, J. Rougier, N. Schön, F. Lindgren, and J. Bamber. Multivariate spatio-temporal modelling for assessing Antarctica’s present-day contribution to sea-level rise. *Environmetrics*, 26(3): 159–177, 2015.
- J. Y. Zhu, C. Sun, and V. O. Li. An extended spatio-temporal Granger causality model for air quality estimation with heterogeneous urban big data. *IEEE Transactions on Big Data*, 3(3):307–319, 2017.